Self-renewing resident cardiac macrophages limit adverse remodeling following myocardial infarction

Sarah A. Dick[1,2,11], Jillian A. Macklin[1,2,3,4,11], Sara Nejat[1,11], Abdul Momen[1], Xavier Clemente-Casares[1], Marwan G. Althagafi[1,4], Jinmiao Chen[5,6], Crystal Kantores[1], Siyavash Hosseinzadeh[1,4], Laura Aronoff[1,4], Anthony Wong[1,7], Rysa Zaman[1,7], Iulia Barbu[1,7], Rickvinder Besla[1,4], Kory J. Lavine[8], Babak Razani[8,9], Florent Ginhoux[5,6], Mansoor Husain[1,2,3,4,10], Myron I. Cybulsky[1,4,10], Clinton S. Robbins[1,4,7,10] and Slava Epelman[1,2,3,4,7,10]★

Macrophages promote both injury and repair after myocardial infarction, but discriminating functions within mixed populations remains challenging. Here we used fate mapping, parabiosis and single-cell transcriptomics to demonstrate that at steady state, TIMD4+LYVE1+MHC-II^lo CCR2− resident cardiac macrophages self-renew with negligible blood monocyte input. Monocytes partially replaced resident TIMD4−LYVE1−MHC-II^hi CCR2− macrophages and fully replaced TIMD4−LYVE1−MHC-II^hi CCR2+ macrophages, revealing a hierarchy of monocyte contribution to functionally distinct macrophage subsets. Ischemic injury reduced TIMD4+ and TIMD4− resident macrophage abundance, whereas CCR2+ monocyte-derived macrophages adopted multiple cell fates within infarcted tissue, including those nearly indistinguishable from resident macrophages. Recruited macrophages did not express TIMD4, highlighting the ability of TIMD4 to track a subset of resident macrophages in the absence of fate mapping. Despite this similarity, inducible depletion of resident macrophages using a *Cx3cr1*-based system led to impaired cardiac function and promoted adverse remodeling primarily within the peri-infarct zone, revealing a nonredundant, cardioprotective role of resident cardiac macrophages.

I schemic cardiovascular disease remains the leading cause of mortality worldwide[1]. After a myocardial infarction, an inflammatory response is directed to the site of injury, resulting in structural and biochemical changes that can lead to adverse cardiac remodeling and dysfunction manifesting clinically as heart failure[2]. Macrophages are specialized mononuclear phagocytes that reside in all tissues from the earliest stages of development and have particularly important roles in the response to injury[3–6]. The mammalian neonatal heart has a remarkable capacity to fully regenerate after injury[7]. Clodronate liposomal depletion of neonatal macrophages prevents regeneration, in part through macrophage-specific expression of growth factors such as IGF-1 and other mechanisms yet to be characterized[8–10]. After ischemic injury in adult mice, both excessive numerical expansion of macrophages[8,11] and nonselective depletion of macrophages[12] limit cardiac repair through excessive inflammatory tissue damage and impaired scar formation, respectively. Macrophage composition in tissue is both heterogeneous at steady state and highly dynamic after injury. Within the adult heart, the majority of resident cardiac macrophages originate from embryonic development, both from early embryonic day 8.5 (E8.5) erythromyeloid progenitors and also later from fetal monocytes[5]. The relative contributions of erythromyeloid progenitor cell–derived fetal liver monocytes and emerging hematopoietic stem cell–derived mono-

cytes to the adult CD64+ cardiac macrophage pool are not known. However, after birth, the slow recruitment of invading monocyte-derived macrophages from circulation leads to competition for tissue residency, and it is not clear whether monocyte-independent populations remain[13].

Circulating monocytes express CCR2, a chemokine receptor important for migration[14], and are enriched in components of the NLRP3 inflammasome. After tissue injury, CCR2+ monocytes and macrophages can produce IL-1β[5], a pro-inflammatory cytokine that promotes cardiovascular disease[15]. In contrast, resident CCR2− macrophages are primarily of embryonic origin and promote angiogenesis and cardiomyocyte proliferation, similar to neonatal macrophages[8,9,16]. However, beyond these observations, more-detailed understanding of cardiac macrophage heterogeneity is lacking.

Here we investigated cardiac macrophage heterogeneity at steady state, plasticity after infarction and the role of resident macrophages in repair. Through the combined use of genetic fate mapping, long-term parabiosis studies and single-cell RNA sequencing (scRNA-seq), we observed that the healthy adult myocardium contains four populations of macrophages, including a subset that is maintained independently of blood monocytes (TIMD4+LYVE1+MHC-II^lo CCR2−), a subset that is partially replaced by monocytes

(TIMD4⁻LYVE1⁻MHC-II^hiCCR2⁻) and two CCR2⁺MHC-II^hi subsets that are fully replaced by monocytes. Ischemic injury induced great diversification of these macrophage subsets. After myocardial infarction, the phosphatidylserine receptor TIMD4[17] and CCR2 emerged as mutually exclusive markers of resident macrophages and recruited macrophages, respectively. Resident macrophage abundance within the infarct zone was markedly reduced after infarction and slowly increased through in situ proliferation. Depletion of diphtheria toxin receptor–labeled resident (*Cx3cr1*-expressing) macrophages promoted adverse cardiac remodeling primarily in the peri-infarct zone, a vulnerable region surrounding infarct tissue. Despite the ability of a small portion of recruited, monocyte-derived macrophages to assume a nearly identical transcriptional fate to the resident macrophage populations, resident cardiac macrophages had nonredundant, spatially localized cardioprotective functions.

Results

Single-cell analyses show unique cardiac macrophage subsets. Flow cytometric analysis of cardiac CD45⁺CD64⁺CD11b⁺ macrophages revealed a single CCR2⁻MHC-II^lo macrophage subset in neonatal mice at post-natal day 14 (P14), whereas in adult mice (>12 weeks old), we detected additional CCR2⁺MHC-II^hi and CCR2⁻MHC-II^hi macrophage populations (Fig. 1a). To quantify monocyte dependence, we paired *Ccr2*⁻/⁻ mice (*Rosa26*⁺/⁺), which lack circulating Ly6C^hi monocytes, with *Ccr2*⁺/⁺ mice, which carried a constitutively expressed gene encoding the membrane-localized TdTomato (Td) reporter in the *Rosa26* locus (*Rosa26*^mTmG/mTmG; *R26*^mTmG), for 6 months. Cardiac tissue from the *Ccr2*⁻/⁻ mice indicated that most CCR2⁺ macrophages (>80%) and a smaller percentage of CCR2⁻MHC-II^hi macrophages (~25%) within the heart were replaced with macrophages derived from *Ccr2*⁺/⁺ (Td⁺) monocytes in circulation, whereas CCR2⁻MHC-II^lo macrophages had little replacement (~12% Td⁺; Fig. 1b).

The heart also contains heterogeneous populations of conventional dendritic cells (cDC1 and cDC2)[18,19] that can express macrophage markers. To characterize mononuclear phagocyte heterogeneity, we sorted cardiac CD45⁺CD64⁺CD11b⁺ macrophages and CD45⁺CD64⁻CD11c⁺MHC-II^lo-hi dendritic cells from adult mice, pooled them in a 1:1 ratio (Supplementary Fig. 1a) and performed scRNA-seq on 1,780 cells using the 10x Genomics platform. t-distributed stochastic neighbor embedding (t-SNE) dimensionality reduction analysis identified 11 major macrophage and dendritic cell clusters (Fig. 1c–e). To validate cluster identity, we used the top ~30 cluster-defining genes (Fig. 1d) to generate a similarity score to all mononuclear phagocyte populations found in the ImmGen[20] data repository (Supplementary Fig. 1b). We confirmed four macrophage clusters (clusters 1, 2, 3 and 5), one monocyte cluster (cluster 4), two cDC clusters (CD209a cDC2, cluster 9; and XCR1 cDC1, cluster 8) and one cluster of dendritic cells (DC#3, cluster 9) resembling dendritic cells found in secondary lymphoid organs. Macrophages and dendritic cells in cell cycle were defined by cell cycle–specific genes[21] in a subcluster containing cDC1s (cluster 10a) and a mixed subcluster containing both macrophages and dendritic cells (cluster 10b). Lastly, we observed one myeloid antigen-presenting cell cluster (cluster 6) that expressed some macrophage and dendritic cell genes (*Adgre1*, *C1qc*, *C1qa*, MHC-II genes and *Itgax*) but not lineage-defining genes (*Fcgr1*, *Maf*, *Mertk*, *Dpp4*, *Flt3* or *Zbtb46*)[22,23] and did not have high expression of plasmacytoid dendritic cell genes (*Siglech*, *Bst2*, *Ly6c2* or *Irf8*) (Fig. 1d and Supplementary Fig. 1b,c). Of the macrophage clusters, cluster 1 expressed genes such as *Timd4*, *Lyve1* and *Igf1* and was the most transcriptionally unique macrophage cluster (termed the *Timd4* cluster; Fig. 1f). Cluster 2 had relatively higher expression of antigen-presentation genes (such as *H2-eb1*) and was correlated with CCR2⁻MHC-II^hi macrophages (termed the *Mhc-II* cluster). Macrophages in cluster 3 were identified as CCR2⁺ macrophages (termed the *Ccr2* cluster).

Cluster 5 was enriched in many interferon-stimulated genes such as *Irf7*, *Isg20* and *Ifit1* (termed the *Isg* cluster; Fig. 1d,f).

We performed pathway analysis by individually comparing the *Timd4* cluster to other clusters. *Timd4* cluster pathways were focused on homeostatic and regenerative functions; that is, endocytosis, lysosome function, angiogenesis and regeneration (Fig. 1g). Relative to the *Timd4* cluster, translational-ribosomal pathways were strongly upregulated in the *Mhc-II*, *Ccr2* and *Isg* clusters, whereas classic inflammatory pathways, including respiratory burst, response to interleukin 12, interferon-γ and type I interferon, were enriched in the *Ccr2* and *Isg* clusters (Fig. 1g). These data reveal the existence of unique, cluster-specific functions in macrophages at steady state.

Single-cell trajectories reveal developmental relationships. To determine whether hypothetical developmental relationships exist between monocytes and macrophage clusters, we reclustered these populations (clusters 1–5) to provide trajectories of single cell–based changes in gene expression (Fig. 2a). Seurat-defined clusters were superimposed on a pseudotime trajectory produced by the Monocle[24] algorithm, which revealed that macrophages in the *Timd4* cluster occupied a separate trajectory branch (B1; Fig. 2b). Monocytes and macrophages found in the *Ccr2* and *Isg* clusters occupied a second branch (B2; Fig. 2b), whereas macrophages in the *Mhc-II* cluster straddled all three branches (B3; Fig. 2b). The Mpath[25] algorithm demonstrated similar ordering, suggesting that macrophages in the *Isg* cluster could arise from the *Ccr2* cluster, rather than monocytes (Fig. 2c), which was confirmed by a restricted Monocle analysis (Fig. 2d).

Gene expression was then plotted as a function of pseudotime in Monocle to track changes across different macrophage states. *Klf2*, *Mafb* and *Maf* expression was low in the *Ccr2* cluster, higher in the *Mhc-II* cluster and even greater in the *Timd4* cluster (Fig. 2e,f), suggesting that these transcription factors tracked with cardiac macrophage fate. Loss of expression of the *Mhc-II* cluster genes *Cx3cr1* and *Il1b* was associated with gain of *Timd4*, *Lyve1* and *Igf1* expression in the *Timd4* cluster (Fig. 2e,f), which was the most transcriptionally distinct subset. In contrast, the *Ccr2*, *Mhc-II* and *Isg* clusters seemed to make up a spectrum of related lineages, with the *Isg* cluster adopting a unique activation state focused around type I interferon signaling. Tracking gene expression changes across macrophage states revealed coordinated patterns defining macrophage subset identification and functions.

***Cx3cr1*-based mapping tracks resident cardiac macrophage fate.** To track cardiac macrophages that are maintained independently of blood monocytes, we used a mouse line with tamoxifen-inducible *Cx3cr1*^CreERT2–IRES–YFP (termed *Cx3cr1*^CreER-YFP) controlled by the endogenous *Cx3cr1* promoter[26] crossed with *Rosa26*-stop-TdTomato reporter mice (termed *Cx3cr1*^CreER-YFP:*R26*^Td; Fig. 3a). Earlier studies have shown robust tamoxifen-inducible reporter gene expression in *Cx3cr1*-expressing resident macrophages and transient labeling of blood monocytes[13,26,27]. We fed tamoxifen-containing chow to 3-week-old mice for 10 d, followed by normal chow for 1–10 weeks. Labeling of CD115⁺CD11b⁺Ly6c⁺ blood monocytes before tamoxifen administration was negligible (<0.2% Td⁺). Ly6c⁺ blood monocytes were efficiently labeled (92–95% Td⁺) immediately after tamoxifen administration, and labeling returned to baseline 2–3 weeks after tamoxifen discontinuation (<0.5%; Fig. 3b). More than 90% of total CD11b⁺CD64⁺ cardiac macrophages were Td⁺ immediately after tamoxifen administration (Fig. 3b). Over a 5-week period, CCR2⁻ cardiac macrophages retained Td expression, whereas CCR2⁺ cardiac macrophages gradually lost Td expression after tamoxifen discontinuation (Fig. 3b), consistent with replacement of CCR2⁺ macrophages by unlabeled monocytes. To further assess macrophage turnover based on scRNA-seq cluster–defining markers, we labeled resident cardiac macrophages
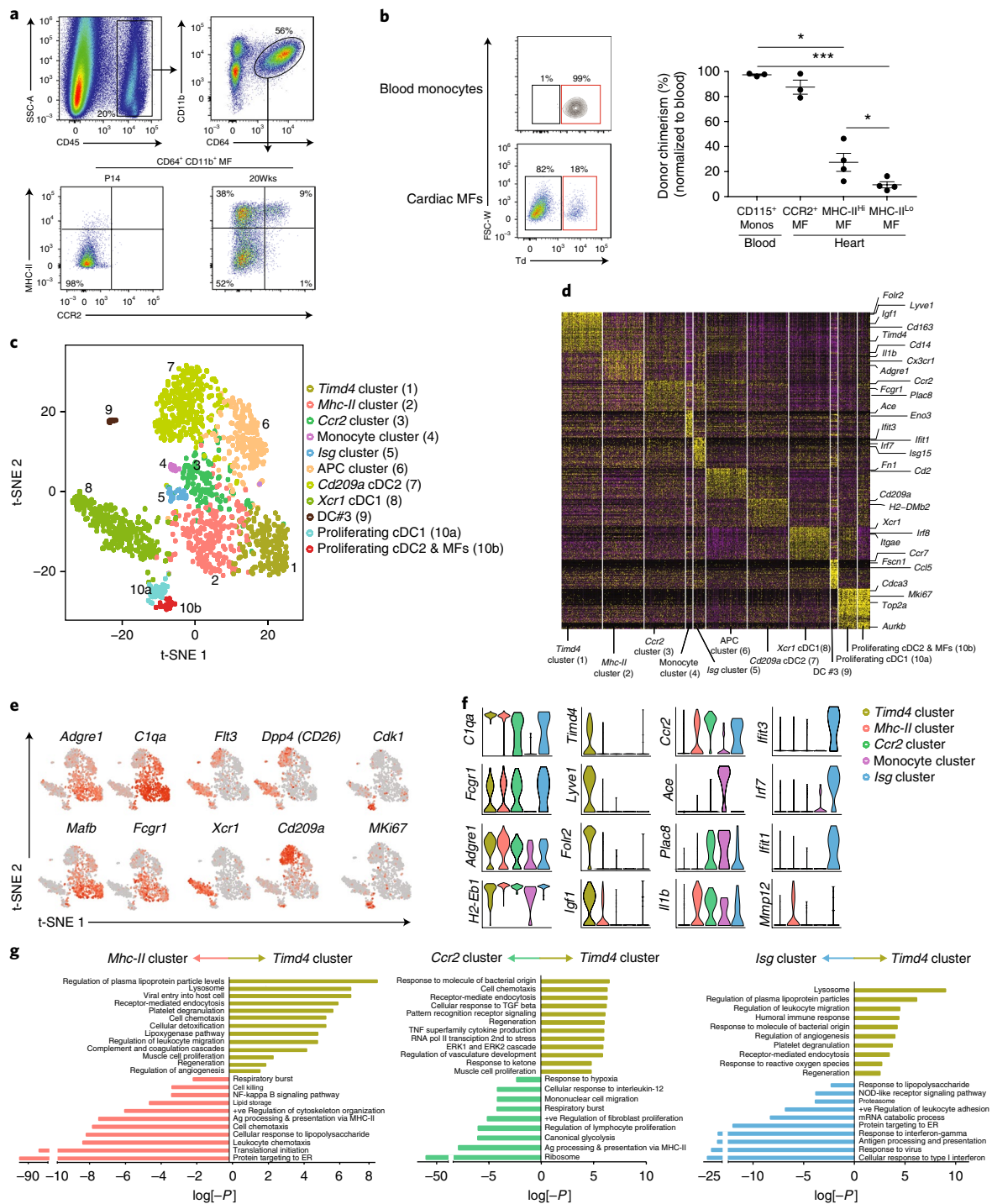
Fig. 1 | Single-cell RNA sequencing reveals distinct cardiac macrophage and dendritic cell subsets at steady state. a, Representative flow plots of the gating scheme used to identify total cardiac macrophages (SCC-A, side scatter area). Live, CD45+CD64+CD11b+ cells were further parsed based on expression of CCR2 and MHC-II from neonate (P14) and adult (20-week-old) mice; experiment was repeated independently five times with similar results. **b**, Parabiosis was performed on 8-week-old recipient *Ccr2−/−* mice that were paired with *Ccr2+/+:R26mTmG/mTmG* donor mice for 6 months. Donor chimerism was determined in blood CD115+CD11b+ monocytes (Monos) and CD64+CD11b+ cardiac macrophages (MF) in the recipient *Ccr2−/−* mouse (FSC-W, forward scatter width). Tissue chimerism (percentage Td+) was quantified and normalized to blood monocyte chimerism (graph; right). *n* values (left to right): 3, 3, 4, 4. *P < 0.05, ***P < 0.001; two-tailed Student's *t*-test; center value, mean; error bars, s.e.m.; experiment was repeated twice. **c**, Sorted cardiac CD45+CD64+CD11b+ macrophages and CD45+CD64−CD11c+MHC-IIlo-hi dendritic cells from adult mice were pooled in a 1:1 ratio; transcriptomic analysis on 1,780 individual cells was performed using the 10x Genomics platform. t-SNE dimensionality reduction analysis identified 11 major clusters. **d**, Heatmap of the 65 most differentially expressed genes in each cluster from Fig. 1c. **e**, Feature plots depicting single-cell gene expression of individual genes. **f**, Violin plots of cluster-defining genes (clusters 1–5). **g**, Differentially expressed genes in the *Timd4* cluster were compared to the *Mhc-II* cluster, the *Ccr2* cluster and the *Isg* cluster using gProfiler. Pathway enrichment is expressed as the log[−P] adjusted for multiple comparison. ER, endoplasmic reticulum.
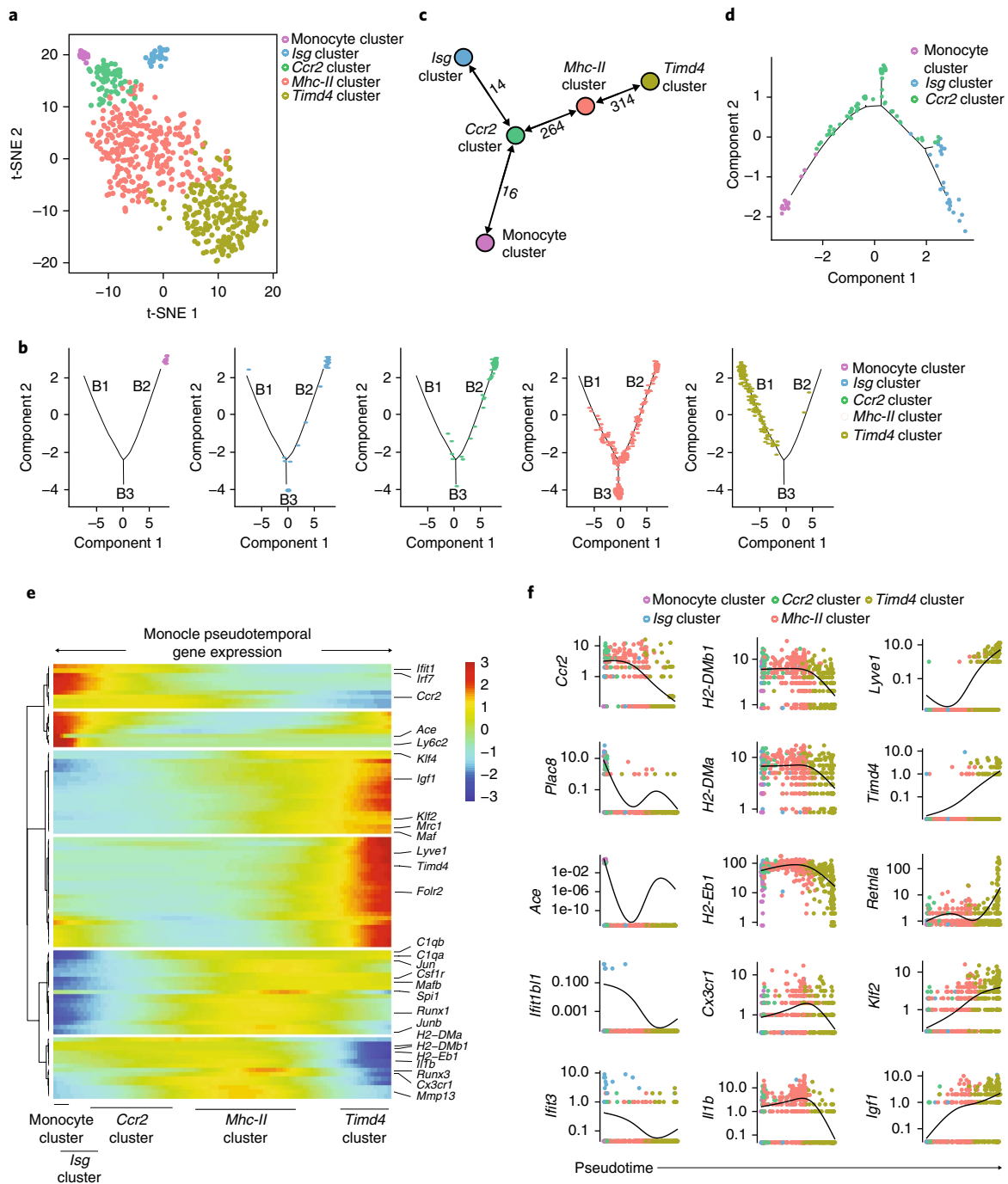
Fig. 2 | High-dimensional single-cell mapping and trajectory analysis reveals four macrophage clusters that occupy distinct activation states. a, Cells found in clusters 1–5 (Fig. 1d, including the *Timd4* cluster, the *Mhc-II* cluster, the *Ccr2* cluster, the *Isg* cluster and monocytes) were reclustered using Seurat. **b,c**, Differentially expressed genes between clusters were used to generate hypothetical developmental relationships using both Monocle (**b**) and Mpath (**c**) algorithms. **b**, B1–B3 represent individual branches in Monocle. **c**, Numbers between nodes are the absolute number of transitioning cells between two populations and highlight the strength of relationship between two subsets. **d**, Focused Monocle trajectory analysis including only the monocyte cluster, *Ccr2* cluster and *Isg* cluster. **e**, Heatmap of differentially expressed genes, ordered based on their common kinetics through pseudotime using Monocle. The relative position of individual Seurat-based clusters across pseudotime is depicted below. **f**, Cluster-defining gene expression plotted as a function of pseudotime, with Seurat's original cluster colors (**a**) superimposed.

(as in Fig. 3b) and analyzed them 20 weeks after tamoxifen discontinuation. CCR2−MHC-IIloTIMD4+ cardiac macrophages retained high Td reporter expression (~90% Td+) after tamoxifen discontinuation and had very little donor chimerism (~2%) in parabiotic studies (Fig. 3c,d). The other two subsets had progressively higher turnover. CCR2−MHC-IIhiTIMD4− macrophages were ~75%

Td+, with ~20% chimerism by parabiosis, whereas CCR2+MHC-IIhiTIMD4− macrophages were about 15–20% Td+, with almost complete chimerism (~90%) in parabiotic studies (Fig. 3c,d). Thus, CCR2 expression alone identified a subset of cardiac macrophages that were fully replaced by blood monocytes in adult mice, and by stratifying the remaining macrophages by TIMD4
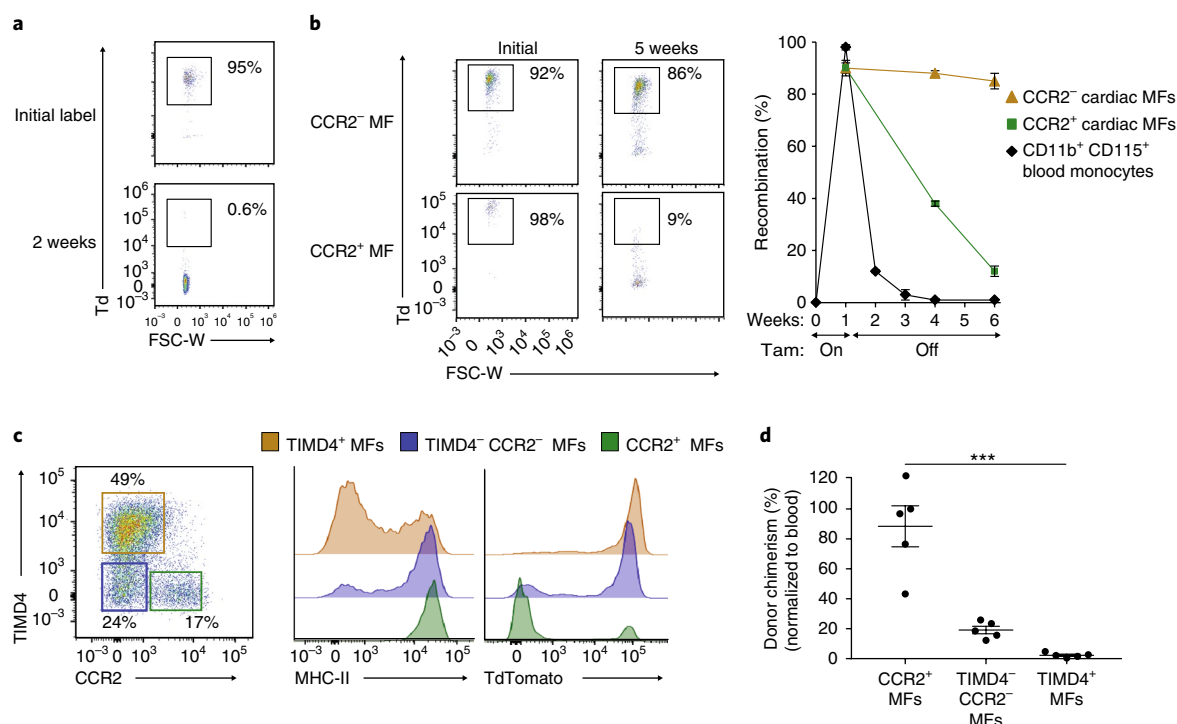
Fig. 3 | TIMD4 and CCR2 are durable markers of resident and recruited macrophages. a,b, 3-week-old $Cx3cr1^{CreER-YFP}$:$R26^{Td}$ mice were fed tamoxifen (Tam)-containing chow for 10 d and then were analyzed after tamoxifen discontinuation (0–20 weeks). Recombination rates are expressed as percentage Td+ cells among blood CD115+CD11b+ monocytes 2 weeks (**a**) and 5 weeks after tamoxifen discontinuation in cardiac CD11b+CD64+CCR2+MHC-IIhi and CD11b+CD64+CCR2- macrophages (**b**). $n = 5$; center value, mean; error bars, s.e.m. Experiment was repeated independently twice with similar results. **c,** At 20 weeks after tamoxifen discontinuation, total cardiac macrophages were stratified into three populations based on expression of CCR2 and TIMD4, wherein MHC-II and TdTomato reporter expression was assessed. Experiment was repeated independently five times with similar results. **d,** Cardiac macrophages were isolated from parabiotic pairs (CD45.2:CD45.1) to determine donor chimerism after 9 weeks of pairing in the three populations outlined in Fig. 3c. Chimerism rates for cardiac macrophages were normalized for blood monocyte chimerism. $n = 5$. ***$P < 0.001$; two-tailed Student's t-test; center value, mean; error bars, s.e.m.; one experiment.

and MHC-II, we identified macrophage subsets with limited monocyte dependence.

Next we examined Td reporter expression in tissue macrophages in $Cx3cr1^{CreER-YFP}$:$R26^{Td}$ mice from birth to adulthood without tamoxifen or with tamoxifen injected at E18.5. In the absence of tamoxifen, Td+ macrophages were detected in resident macrophage populations that express $Cx3cr1$ immediately after birth (that is, microglia and cardiac macrophages) (Supplementary Fig. 2a). Background Td expression reached a relative plateau of ~25% of total cardiac macrophages between 8 weeks and 13 weeks of age. Tissue macrophages with low expression of $Cx3cr1$ (such as liver Kupffer cells) had very low Td expression (0–5%), and there was virtually no Td expression in blood monocytes at any time point examined (E18.5, 35 weeks of age) in the absence of tamoxifen. 11-week-old mice treated with tamoxifen at E18.5 had high Td expression in brain microglia (~99%) and cardiac macrophages (~80%) and lower expression in liver Kupffer cells (~40%; Supplementary Fig. 2a). We also observed similar Td reporter expression in the absence of tamoxifen in cardiac macrophages and brain microglia from an independently generated $Cx3cr1^{CreERT2}$ line[27] bred to the same $R26^{Td}$ reporter (Supplementary Fig. 2b).

To investigate whether monocyte-derived macrophages could be induced to express the Td reporter, we isolated Td- bone marrow from adult CD45.2+ $Cx3cr1^{CreER-YFP}$:$R26^{Td}$ mice and reconstituted sublethally irradiated CD45.1+ recipients. At 6 weeks after reconstitution, CD45.2+ monocytes and monocyte-derived cardiac CD45.2+ macrophages were Td- (~98%; Supplementary Fig. 2c), indicating that $Cx3cr1^{CreER-YFP}$:$R26^{Td}$ monocytes do not

induce the expression of the Td reporter upon macrophage differentiation in the absence of tamoxifen. Thus, although some macrophage populations in $Cx3cr1^{CreER-YFP}$:$R26^{Td}$ expressed Td in the absence of tamoxifen administration, Td reporter activity reliably distinguished resident cardiac macrophages from recruited, monocyte-derived macrophages.

Resident macrophages are lost within infarcted myocardium. To examine resident macrophage dynamics during sterile injury, we used a model of myocardial infarction through surgical ligation of the left anterior descending artery[5]. Cardiac tissue was analyzed by flow cytometry at different times after injury in the ischemic zones (infarct and peri-infarct tissue) and the remote (noninfarcted) zones of $Cx3cr1^{CreER-YFP}$:$R26^{Td}$ mice fed tamoxifen at 3 weeks of age for 10 d (Fig. 4a). Tamoxifen was discontinued for 6 weeks before mice were infarcted. The absolute number of resident Td+ macrophages in the ischemic zone was reduced by ~60% after infarction (day 2) compared to noninfarcted mice (Fig. 4b), including both resident CCR2-MHC-IIloTIMD4+ and CCR2-MHC-IIhiTIMD4- macrophages (Supplementary Fig. 3a). Absolute numbers of resident Td+ macrophages slowly increased after infarction (days 4–28), compared to day 2, whereas the number of recruited Td- macrophages decreased. However, the ratio of resident macrophages to recruited macrophages did not return to preinfarct levels by 4 weeks after infarction (Fig. 4c,d). Resident CCR2-MHC-IIhiTIMD4- macrophages were ~75% Td+ at steady state, but after infarction, only ~5% remained Td+, indicating that recruited macrophages made up the vast majority (Fig. 4e). In contrast, resident
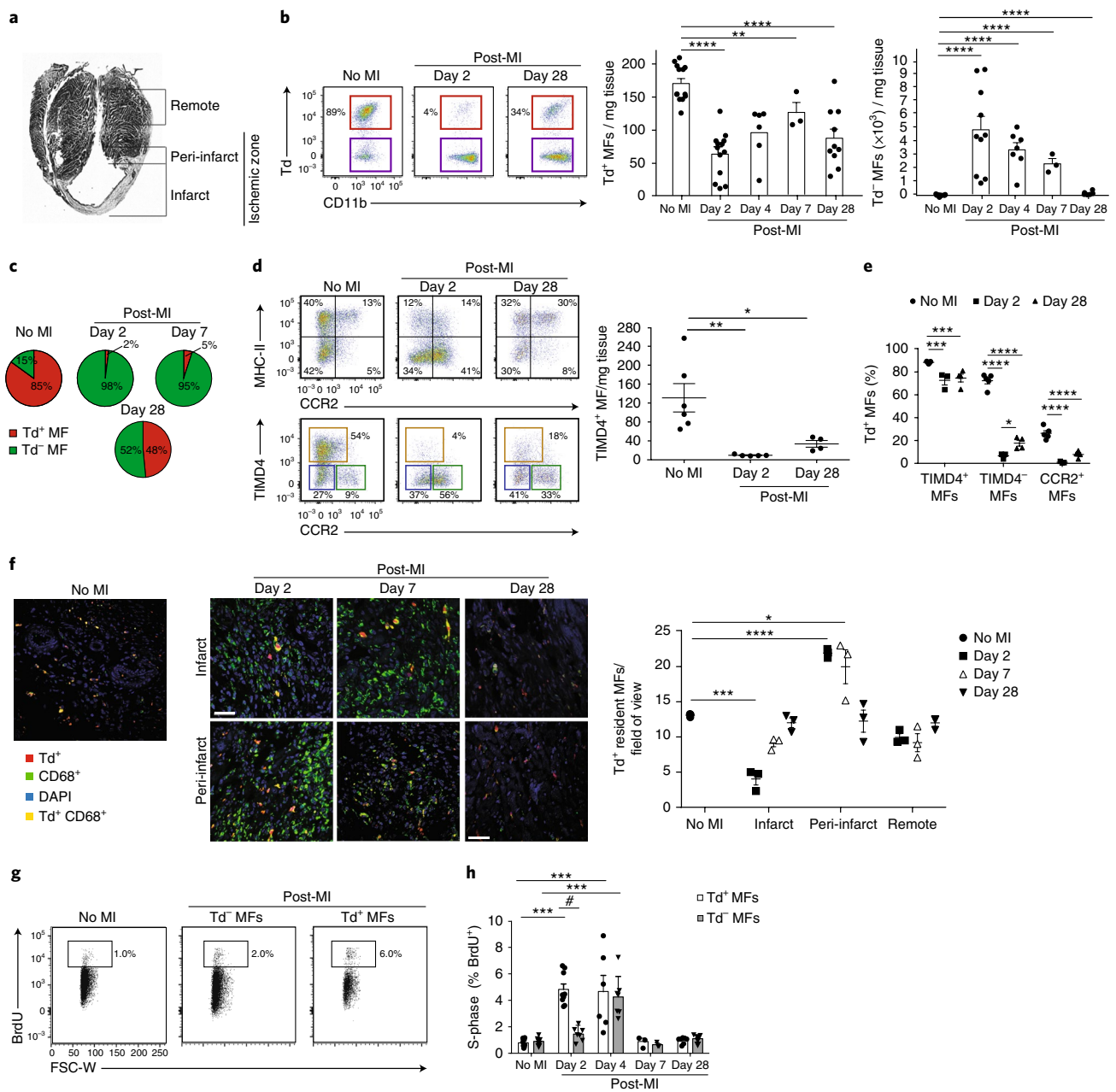
Fig. 4 | Resident macrophages are lost in infarcted cardiac tissue and return via local proliferation. 3-week-old *Cx3cr1*[CreER-YFP]:*R26*[Td] mice were fed tamoxifen-containing chow for 10 d and then underwent left anterior descending artery ligation to induce a myocardial infarction (MI) 6 weeks after tamoxifen discontinuation. **a**, Fixed frozen cardiac tissue section demonstrating the infarct zone, peri-infarct zone and noninfarcted (remote) left ventricular myocardium. The ischemic zone, containing both infarct and peri-infarct regions, was analyzed in all flow cytometric experiments together. **b**, Cardiac tissue was isolated at different time points after MI from the ischemic zone; representative flow cytometric analysis of resident CD64+CD11b+Td+ macrophages is shown (left). Adjacent graphs (right) quantify resident CD64+CD11b+Td+ and recruited CD64+CD11b+Td− macrophages per mg of cardiac tissue; *n* values (left to right throughout): Td+,13, 13, 6, 3, 10;Td−,12, 10, 7, 3, 6. Experiment was repeated three times for day 2, twice for days 4 and 28, once for day 7 and six times for control with similar results. Two-tailed Student's *t*-test compared with control, corrected with Bonferroni. **c**, Td+ and Td− cardiac macrophages, presented as a percentage of total macrophages, at indicated times post-MI based on Fig. 4b. **d**, Flow plots of CD64+CD11b+ cardiac macrophages stratified by MHC-II versus CCR2, or TIMD4 versus CCR2 post-MI; TIMD4+ macrophages quantified per mg of tissue (graph, right). *n* = 6, 5, 4. Experiment was repeated twice. One-way ANOVA adjusted for multiple comparisons. **e**, Percentage of Td+ macrophages determined at each time point after MI within three populations outlined in Fig. 3d. *n* = 5, 3, 4. Experiment was repeated twice. Two-way ANOVA adjusted for multiple comparisons. **f**, Representative immunofluorescence images of cardiac tissue after MI. Cardiac CD68+ macrophages were identified as Td+ resident macrophages or Td− recruited macrophages in the infarct, peri-infarct and remote regions; total number of such cells was quantified (graph, right) from five individual images per region per mouse. *n* = 3. Two-tailed unpaired Student's *t*-test. One experiment. **g,h**, Representative flow cytometric plots of CD64+CD11b+ cardiac macrophages isolated 2 d after MI from the ischemic zone. Mice were injected (i.p.) with BrdU 2 h before isolation to label all cells in S-phase of cell cycle. The percentage of BrdU+ cells was quantified in the Td+ resident macrophage and Td− recruited macrophage subsets, compared with that of animals with no MI (**h**). *n* = 10, 8, 9, 7, 7, 7, 3, 3, 7, 7. Experiment was repeated three times for day 2, twice for days 4 and 28, once for day 7 and six times for control. Two-tailed Student's *t*-test compared with control, corrected with Bonferroni. For all: *P < 0.05, **P < 0.01, ***P < 0.001, ****P < 0.0001. Center value, mean; error bars, s.e.m.

CCR2⁻MHC-IIˡᵒTIMD4⁺ macrophages were ~90% Td⁺ at baseline, and after infarction they remained at ~75% Td⁺ at days 2 and 28 (Fig. 4e), indicating that TIMD4 expression was maintained on resident Td⁺ macrophages and recruited macrophages did not become TIMD4⁺, even at 28 d after infarction.

Immunofluorescence imaging also indicated a 70% loss of Td⁺ cardiac macrophages in the infarct zone at day 2 after infarction, compared to noninfarcted hearts, with a progressive increase in density over 28 d (Fig. 4f). Increased resolution of the infarct region versus the peri-infarct region demonstrated a region-specific increase in the absolute number of Td⁺ cardiac macrophages in the peri-infarct zone at days 2 and 7 after infarction, compared to control noninfarcted heart tissue. LYVE1 was coexpressed on TIMD4⁺ macrophages, as determined by flow cytometry (Supplementary Fig. 3b), and was highly expressed within the *Timd4* cluster, as determined by scRNA-seq (Fig. 1f). We partitioned resident macrophages into CD68⁺LYVE1⁺Td⁺ and CD68⁺LYVE1⁻Td⁺ macrophages in the cardiac tissue sections (Supplementary Fig. 3c). LYVE1⁻Td⁺ macrophages increased in number in the peri-infarct zone at day 2 after myocardial infarction, compared to noninfarcted control, whereas the number of LYVE1⁺ Td⁺ macrophages did not change (Supplementary Fig. 3c), highlighting spatial enrichment of resident LYVE1⁻ macrophages in the peri-infarct zone.

We assessed macrophage proliferation in vivo after infarction by administering BrdU intraperitoneally (i.p.) 2 h before isolation to label cells in S-phase[5]. We observed a proliferative burst in resident Td⁺ cardiac macrophages at days 2 and 4 after infarction, compared to noninfarcted hearts, whereas recruited Td⁻ macrophages exhibited increased proliferation only at day 4 after infarction (Fig. 4g,h). When parsing resident Td⁺ macrophages into TIMD4⁺ and TIMD4⁻ subsets, we observed a slight proliferative advantage of resident Td⁺TIMD4⁻ macrophages (Supplementary Fig. 3d); this supports the observation that the analogous resident Td⁺LYVE1⁻ subset increased in cell number in the peri-infarct region (Supplementary Fig. 3c).

To ensure that Td⁻ blood monocytes did not differentiate into Td⁺ macrophages after recruitment into the cardiac tissue after infarction (in the absence of tamoxifen), we produced chimeric mice in a CD45.1⁺ background that contained CD45.2⁺ *Cx3cr1*^CreER-YFP^:*R26*^Td^ monocytes through either parabiosis (Supplementary Fig. 4a) or bone-marrow transfer after chest wall–shielded irradiation (Supplementary Fig. 4b). Myocardial infarction was induced at 2 weeks after parabiosis or 6 weeks after bone marrow transfer, and cardiac tissue was analyzed by flow cytometry at 5 d or 28 d, respectively, after myocardial infarction. CD45.2⁺ monocytes and monocyte-derived macrophages isolated from CD45.1⁺ mice did not induce Td expression after recruitment post-infarction in the absence of tamoxifen (Supplementary Fig. 4a,b). To confirm tamoxifen responsiveness in these two systems, we assessed CD45.2⁺ macrophages from donor parabiotic mice and bone marrow chimeras injected with tamoxifen before isolation, and both showed large numbers of Td⁺ macrophages. Thus, in the inflammatory environment after irradiation or myocardial infarction, the *Cx3cr1*^CreER-YFP^:*R26*^Td^ line retained the ability to distinguish resident from recruited cardiac macrophages.

Recruited cardiac macrophage plasticity in infarcted tissue. To explore macrophage heterogeneity after ischemic injury, we performed scRNA-seq on CD45⁺CD11b⁺CD64ˡᵒ⁻ʰⁱ macrophages from *Cx3cr1*^CreER-YFP^:*R26*^Td^ mice treated with tamoxifen at E18.5 and infarcted at 7 weeks of age. Macrophages were isolated from the ischemic zone 11 d after infarction (Fig. 5a). At 11 d after myocardial infarction, the acute inflammatory response is resolved and recruited monocytes have differentiated into tissue macrophages[28–30], making it an ideal time point to study macrophage heterogeneity. We sequenced 1,806 cells from control noninfarcted

mice and 4,697 cells from the ischemic zone after infarction. t-SNE analysis of noninfarcted mice revealed six clusters identical to those previously identified (*Timd4* cluster, *Mhc-II* cluster, *Ccr2* cluster, *Isg* cluster, proliferating macrophages and monocytes; Fig. 5b). In macrophages isolated from infarcted tissue, we identified 13 clusters, 6 of which precisely overlapped the 6 clusters identified in noninfarcted hearts, and 7 clusters were unique to infarcted tissue (Fig. 5b). Approximately 64% of the macrophages sequenced after infarction fell in unique clusters (Fig. 5b,c), indicating that the majority of macrophages evolved distinct transcriptional signatures compared to noninfarcted tissue.

Post-infarct macrophages from individual overlapping clusters had nearly identical gene expression patterns compared to macrophages of the same cluster in the noninfarcted control sample, except for a total of 67 genes (sum across all overlapping clusters; Fig. 5d,e; Supplementary Fig. 3e and Supplementary Table 1). Genes associated with mature macrophages (*Lyve1*, *Timd4*, *Retnla*, *Cd163*, *Folr2* and *Klf2*) were downregulated, whereas genes associated with monocytes (*Ms4a7* and *Spp1*) were upregulated in post-infarction macrophages, compared to noninfarcted control macrophages (Fig. 5f). Classic macrophage genes (*Adgre1*, *Fcgr1* and *C1qa*) remained unchanged, as did the vast majority (7,543) of other genes detected in each overlapping cluster (Fig. 5d–f). Macrophages expressing the transcript encoding Td were found in control noninfarcted mice at a frequency much lower (~13%) than expected based on flow cytometric analysis (~80% Td⁺, Supplementary Fig. 2a); this limited our ability to track resident populations by scRNA-seq. However, similar to the results obtained from flow cytometric analysis, there was a decrease in both the absolute number and percentage of Td-expressing macrophages in both the post-infarct overlap and post-infarct unique clusters, compared to the noninfarcted clusters (>90% loss of Td-expressing macrophages; Fig. 5g). These data suggest that after infarction, macrophages that were found in overlapping clusters (clusters 1–6) were mainly derived from Td⁻ monocytes, yet they had nearly identical transcriptional signatures as macrophages in steady-state control mice, with the exception of a very small number of core genes found in resident macrophages, such as *Timd4*, *Lyve1*, *Igf1* and *Folr2* (Fig. 5f).

Among the seven unique post-infarct macrophage clusters, differential gene expression analysis and comparison to the ImmGen database identified four macrophage clusters (8–11) and one dendritic cell cluster (7; CD209a cDC2s) (Fig. 5b,c and Supplementary Fig. 3e,f). Compared to the overlapping clusters, macrophages in unique clusters 8–11 were enriched most strongly in inflammatory pathways (response to interferon-γ; monocyte chemotaxis) but also in some reparative pathways (Fig. 5h; Supplementary Table 2 for all cluster-specific genes). Cluster 6 was composed of three subclusters (6a–6c) that clustered separately (Fig. 5b). Monocle trajectory analysis revealed three different fates along the same developmental trajectory, with a progressive increase in the expression of macrophage genes and a reciprocal loss in the expression of monocyte genes (Fig. 5i). We also observed the progressive upregulation of pathways involved in hypoxia (HIF-1α signaling; $P=1.4\times10^{-3}$), glycolytic metabolism ($P=0.02$) and extracellular matrix interactions ($P=1.6\times10^{-3}$) as monocytes transitioned into macrophages (Fig. 5j), consistent with the anaerobic environment of ischemic tissue. Therefore, although recruited macrophages had a high degree of plasticity, they did not adopt the core transcriptional signature of resident populations and could be distinguished by flow cytometry and scRNA-seq.

Cardiac macrophage heterogeneity in human cardiomyopathy. Next we sorted human cardiac CD45⁺CD64⁺CD14⁺ macrophages from subjects with cardiomyopathies. Based on MHC-II (HLA-DR) and CCR2 expression, we identified three subsets, CCR2⁻MHC-IIʰⁱ, CCR2⁺MHC-IIʰⁱ and CCR2⁺MHC-IIˡᵒ (Supplementary Fig. 5a,b),
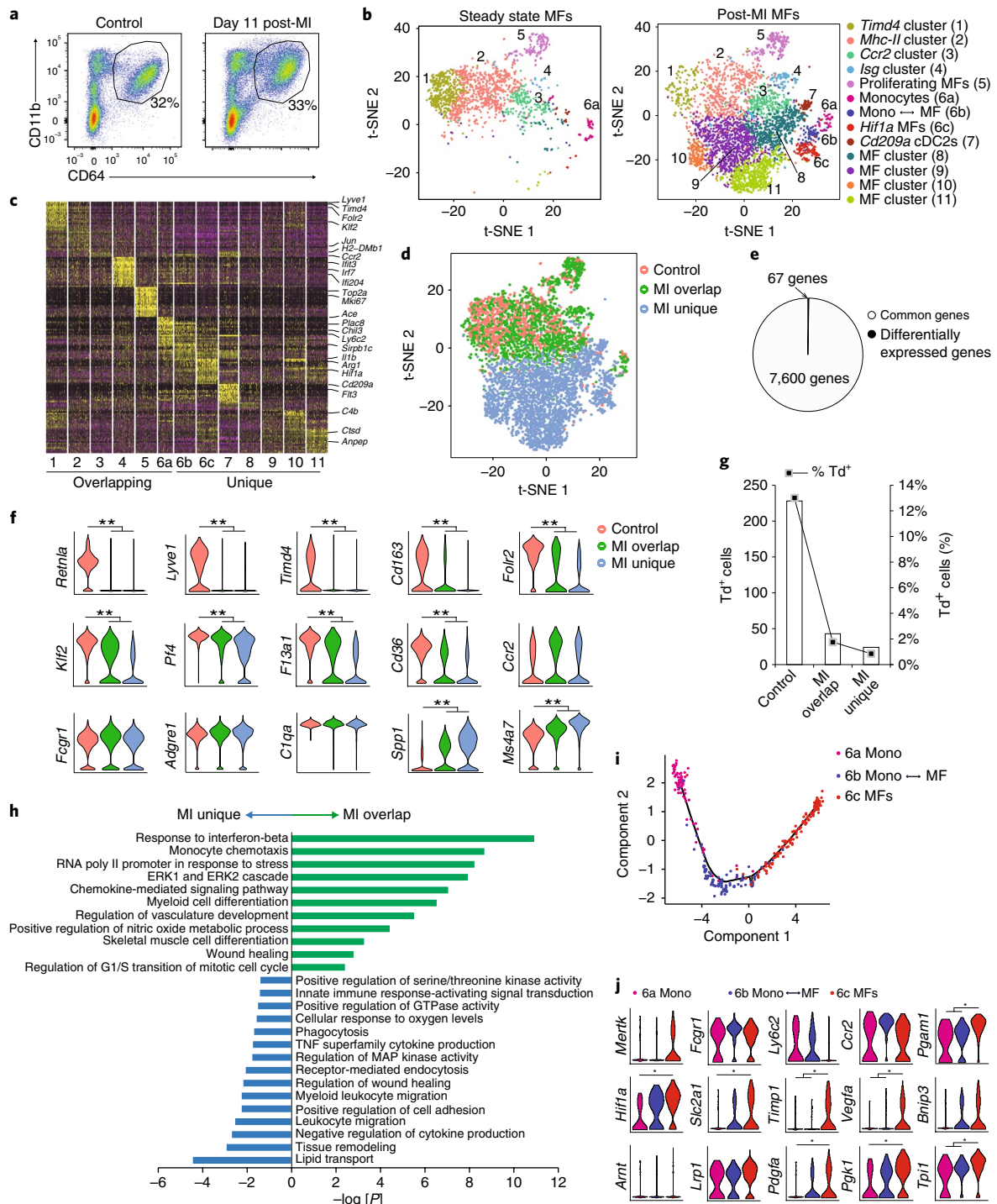
Fig. 5 | High-dimensional analyses reveal plasticity of recruited macrophages to adopt both unique and resident-like transcriptional states within infarcted tissue. Cx3cr1[CreER-YFP]:R26[Td] mice were administered tamoxifen at E18.5. At 7 weeks of age, mice served as either controls (noninfarcted) or received an MI. Cardiac tissue from control mice and from infarcted mice was isolated (ischemic zone, 11 d after MI). **a**, Live cardiac CD45^{+}CD64[Dim–Hi] CD11b^{+} macrophages were sorted and processed for scRNA-seq as in Fig. 1c (1,806 control cells; 4,697 post-MI cells). One experiment, two mice or four mice pooled for the control group and MI group, respectively. **b**, Seurat-based t-SNE analysis of merged control and post-MI samples reveals 'overlapping clusters' present in both control samples and post-MI samples, and 'unique clusters', present only post-MI. **c**, Heatmap of the top 20 differentially expressed genes per cluster post-MI. **d**, t-SNE plot depicting cells in control sample (pink), and cells in MI sample that overlapped control (MI overlap; green) and cells uniquely found after MI (MI unique; blue). **e**, Pie chart illustrating number of differentially expressed genes between control and MI-overlap groups, relative to number of commonly expressed genes between these two groups (see Supplementary Table 1 for differentially expressed genes per cluster). **f**, Representative violin plots of differentially expressed genes among the three populations as defined in Fig. 5d; **$P < 10^{-13}$ (adjusted for multiple comparisons). **g**, Absolute number and percentage of Td-expressing cells in each cluster defined in Fig. 5d. **h**, Pathway analysis (gProfiler) of differentially expressed genes in MI-overlap versus MI-unique populations. Pathway enrichment is expressed as the $-\log[P]$ adjusted for multiple comparison. **i**, A pseudotemporal trajectory (Monocle) analysis of cluster 6 subsets (Fig. 5b) demonstrates a linear developmental progression from cluster 6a (monocyte) to 6c (macrophage). **j**, Violin plots of differentially expressed genes in cluster 6, including HIF-1α and glycolysis pathway genes. *$P < 10^{-2}$. Statistical analysis for scRNA-seq data is described in Methods.

that seemed to be similar to mouse cardiac macrophages. Differentially expressed genes defined by murine t-SNE clusters were used to determine whether sorted human cardiac macrophage populations expressed similar patterns. The human CCR2⁻MHC-II^hi macrophages expressed many genes found in the murine *Timd4* cluster, including *TIMD4*, *LYVE1*, *CD163*, *FOLR2*, *IGF1* and *MAF* (Supplementary Fig. 5c). Murine gene signatures associated with the *Isg* cluster, the *Ccr2* cluster and monocytes were found predominantly in human CCR2⁺MHC-II^lo monocytes and CCR2⁺MHC-II^hi macrophages. Only 226 genes were differentially expressed between human CCR2⁻MHC-II^hi and human CCR2⁺MHC-II^hi macrophages, with the majority (179 genes) upregulated in CCR2⁺MHC-II^hi macrophages (Supplementary Fig. 5c). Pathway analysis indicated that human CCR2⁺MHC-II^hi macrophages were enriched in hematopoietic stem cell lineage genes ($P = 2.8 \times 10^{-6}$), cytokine–cytokine receptor interactions ($P = 4.6 \times 10^{-5}$) and Toll-like receptor signaling ($P = 2.9 \times 10^{-2}$), whereas human CCR2⁻MHC-II^hi cardiac macrophages were enriched in the complement cascade (47 genes upregulated; $P = 4.4 \times 10^{-2}$). Thus, CCR2 defines recruited monocytes and monocyte-derived macrophages in both mouse models and human cardiomyopathy.

Cx3cr1-based depletion post-infarct worsens cardiac function. Next we used *Cx3cr1*^CreER-YFP:*R26*^Td/DTR mice to label resident macrophages with both the Td reporter and the diphtheria toxin receptor (DTR) to selectively deplete resident Td⁺ cardiac macrophages through diphtheria toxin injection without affecting other cell types (Supplementary Fig. 6a,b). Diphtheria toxin injection alone, in the absence of ischemic injury, did not cause any detectable recruitment of neutrophils and macrophages, nor did it cause cardiac fibrosis in wild-type mice that did not contain DTR (Supplementary Fig. 6c). To test the functional role of resident macrophages after infarction, we fed 3-week-old *Cx3cr1*^CreER-YFP:*R26*^Td/DTR mice tamoxifen chow for 10 d, and tamoxifen was discontinued for 6 weeks. Daily diphtheria toxin injections were started 1 d before myocardial infarction to deplete and suppress the numerical recovery of resident cardiac macrophages (Fig. 6a,b). There was no difference in the infarct size or cardiac function at day 7 after infarction in diphtheria toxin–treated *Cx3cr1*^CreER-YFP:*R26*^Td/DTR mice, compared to *Cx3cr1*^CreER-YFP:*R26*^Td/+ mice, which lacked the DTR (Fig. 6c,d). However, global left ventricular systolic function deteriorated between days 7 and 28 after infarction, with increased cardiac hypertrophy, fibrosis and increased late mortality by day 35 after infarction in diphtheria toxin–treated *Cx3cr1*^CreER-YFP:*R26*^Td/DTR mice, compared to *Cx3cr1*^CreER-YFP:*R26*^Td/+ mice (Fig. 6e–i). There was no significant change in the magnitude of the inflammatory response in macrophage-depleted mice, compared to nondepleted (*Cx3cr1*^CreER-YFP:*R26*^Td/+) mice, at day 5 after infarction (Supplementary Fig. 6d), indicating that depletion of resident macrophages did not cause an exaggerated inflammatory response acutely.

Although the absolute number of resident CD64⁺Td⁺ cardiac macrophages was similar between noninfarcted controls and post-infarct hearts in the remote zone at all time points analyzed, there was increased recruitment of monocytes and monocyte-derived CD64⁺Td⁻ macrophages in this area at days 2, 4 and 7 after infarction (Supplementary Fig. 6e). However, CD64⁺Td⁺ resident macrophages proliferated robustly in this region, as determined by BrdU incorporation, at days 2 and 4 after infarction (Supplementary Fig. 6f). Depletion of resident cardiac macrophages led to a decrease in left ventricular systolic function from day 7 to day 28 after infarction in the remote zone of diphtheria toxin–treated *Cx3cr1*^CreER-YFP:*R26*^Td/DTR mice, compared to no change in infarcted nondepleted *Cx3cr1*^CreER-YFP:*R26*^Td/+ mice (Supplementary Fig. 6g). We also observed an increase in cardiomyocyte hypertrophy, but no change in cardiac fibrosis, in the remote zone of depleted compared to nondepleted hearts 35 d after infarction (Supplementary

Fig. 6h,i). These data indicate a spatially restricted, primary role for resident Td⁺ macrophages in the peri-infarct zone to prevent pathological remodeling and the development of global left ventricular dysfunction in the surviving myocardium.

Discussion

Here we describe the transcriptional and functional heterogeneity that exists within the innate immune cell compartment of the murine heart, both at steady state and after myocardial infarction. Through a combination of cell tracking and scRNA-seq, we found that the healthy murine myocardium contains four transcriptionally distinct cardiac macrophage subsets with subset-specific life cycles and function. Resident cardiac macrophages accounted for only 2–5% of the total cardiac macrophages within the infarct zone during the first few weeks after infarction, yet their depletion impaired cardiac function and worsened infarct healing. This is underscored by the observation that nearly identical, recruited macrophages were present at nearly the same time yet did not compensate for resident macrophage depletion. A small number of cluster-specific, resident macrophage genes (such as *Timd4*, *Lyve1* and *Igf1*) were not adopted by recruited macrophages, and these genes could have endowed resident macrophages with critical reparative functions. For instance, the phosphatidylserine receptor TIMD4 is used by macrophages in efferocytosis[17], without which ischemic injury is amplified[31]. LYVE1 binds hyaluronan expressed by smooth muscle cells and has an integral role in vascular homeostasis[32]; therefore, loss of LYVE1⁺ macrophages could disrupt adaptive healing mechanisms. The growth factor IGF1, which is secreted by cardiac macrophages, directly promotes angiogenesis[10]. Alternatively, by the time monocytes become peripherally derived resident macrophages, they might have missed the window of opportunity for providing effective cardioprotective functions. Additional studies using *Cx3cr1*-based strategies to target resident macrophages would shed light on which, if any, of these potential mechanisms are involved.

During neonatal cardiac injury, cardiac macrophages proliferate[5,8]. In contrast, ischemic injury in adult mice reduced the abundance of resident Td⁺ cardiac macrophages within infarcted tissue, presumably through cell death due to anoxia and nutrient deprivation. After infarction, a robust proliferative program was triggered in the remaining resident macrophages, similar to that in neonatal cardiac macrophages. Importantly, the neonatal myocardium did not recruit monocytes in significant numbers; this is fundamentally different than in the adult myocardium[8]. The limited capacity to recruit monocytes in large numbers may be an adaptive mechanism that promotes reparative programs inherent to resident, embryonic-derived macrophages during development. The density of peripherally derived CCR2⁺ cardiac macrophage is correlated with cardiac dysfunction after heart transplantation in humans. In addition, preventing monocyte influx in adult mice has beneficial effects when excessive inflammation drives ischemic injury[33,34]. Paradoxically, our data indicate that inhibiting monocyte influx alone could impair development of monocyte-derived macrophages with reparative functions and prevent replacement of reparative resident populations that are lost during the initial insult.

Understanding the tissue-specific cues that drive monocyte fate selection during ischemic injury will be critical in influencing reparative pathways. However, it remains to be clarified whether the nine macrophage clusters found after infarction specify their fate when they enter the myocardium, whether these clusters are at their final transcriptional destinations, or whether they are part of a continuum. Notably, there is evidence that monocyte fate selection occurs not only in tissues but also in the bone marrow. Hematopoietic stem cells produce lineage-committed monocytes before release into circulation, and these monocyte lineages have distinct tissue functions, presumably through epigenetic changes. For example, Ly6C^lo MSR1⁺CEACAM1⁺ blood monocytes enter the
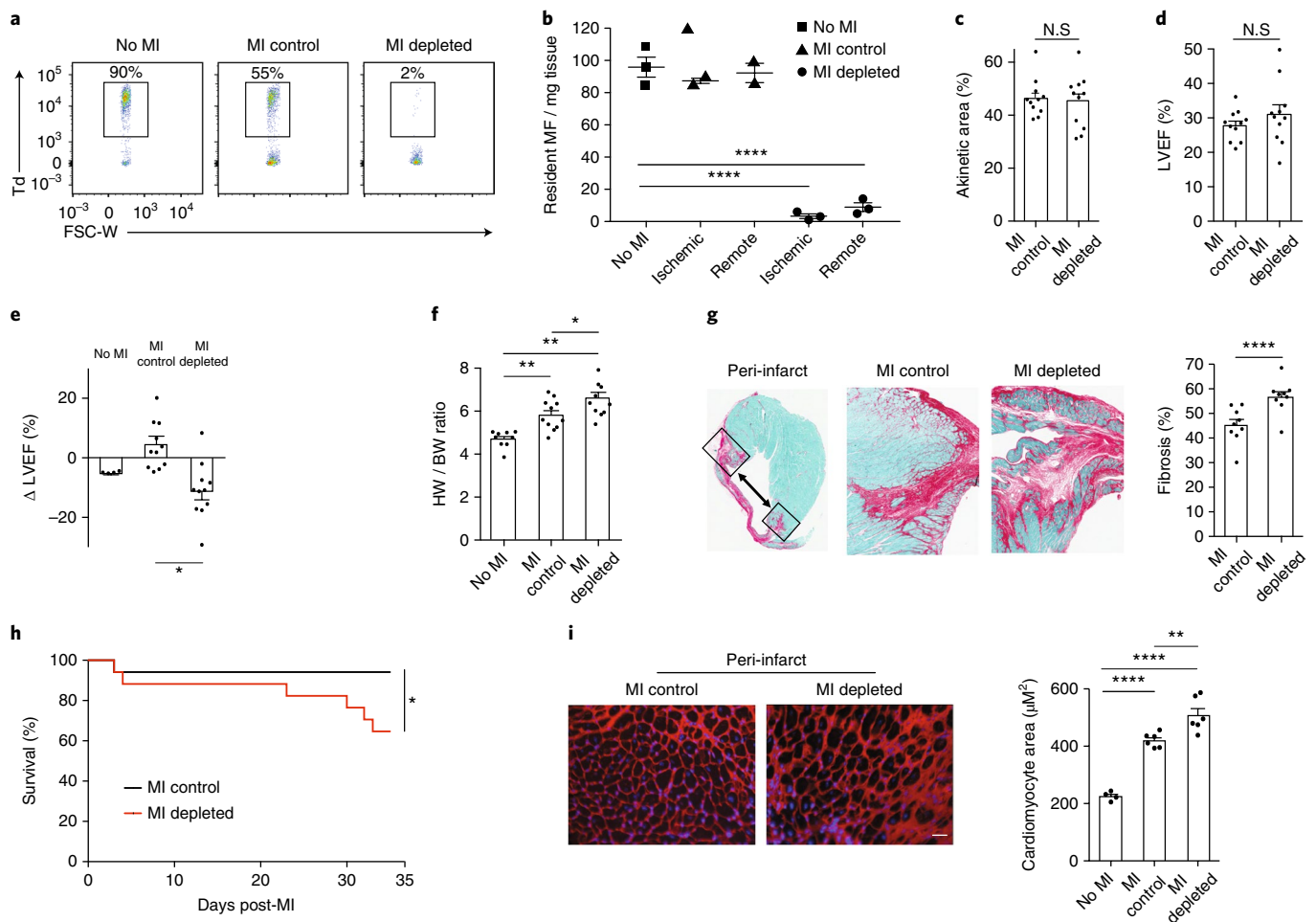
Fig. 6 | Selective depletion of resident cardiac macrophages results in impaired infarct healing and adverse cardiac remodeling primarily within the peri-infarct region. 3-week-old $Cx3cr1^{CreER-YFP}$: $R26^{Td/DTR}$ mice were fed tamoxifen-chow for 10 d, tamoxifen was discontinued for 6 weeks, and mice either were noninfarcted (no MI) or received surgical MI. Mice that received a surgical MI were injected daily with either PBS (MI control) or 250 ng diphtheria toxin (MI depleted), starting the day before surgery. **a,b**, Representative flow cytometric plots (**a**) of CD45$^+$CD64$^+$CD11b$^+$ macrophages, demonstrating the number of Td$^+$ cells remaining at day 35 after infarct within the ischemic zone, and quantified (**b**) in both the ischemic zone and remote zone by flow cytometry per mg of tissue. Resident macrophages were identified as CD64$^+$CD11b$^+$Td$^+$. n values (left to right throughout): 3, 7. Experiment was repeated twice; representative plot is shown. **c**, Infarct size was measured at day 7 after MI by echocardiography, reported as percentage akinetic area. $n = 11$. Experiment was repeated twice with similar results. **d**, Percentage of left ventricular ejection fraction (LVEF) measured at day 7 after MI. $n = 11$. Experiment was repeated twice with similar results. **e**, Average change in ejection fraction from day 7 to day 28 post-MI (ΔLVEF). $n = 4, 11, 11$. Repeated two times with similar results. **f**, Cardiac hypertrophy 35 d after MI, as measured by heart weight (HW) to body weight (BW) ratio. $n = 9, 11, 11$. Experiment was repeated twice with similar results. **g**, Histological cross-section (left) and quantification (right) of the cardiac peri-infarct zone at day 35 after MI. Hearts were scanned at 10× magnification. Percentage fibrotic area was quantified using Fast Green staining and ImageJ analysis, with four images per zone per heart in two sections, 150 μm apart. $n = 9$. Experiment was repeated once. **h**, Kaplan-Meier curve representing percentage survival at day 35 post-MI. $n = 17$. Experiment was repeated twice with similar results. **i**, Cardiomyocyte hypertrophy, assessed with wheat germ agglutinin staining in the peri-infarct zone. Hearts were imaged at 20× magnification and cardiomyocyte area was measured in ImageJ, with eight images per zone per heart at two cutting levels. $n = 4, 6, 6$. Experiment was repeated once. For all: $*P < 0.05$, $**P < 0.01$, $***P < 0.001$, $****P < 0.0001$; Two-tailed Student's t-test; center value, mean; error bars, s.e.m.

lungs and promote tissue fibrosis, Ly6C^{hi}CD209a$^+$ monocytes preferentially differentiate into monocyte-derived dendritic cells[35,36], and immunoregulatory Ym1$^+$Ly6C^{hi} monocytes are released only in the recovery phase after injury and promote tissue repair[37].

Earlier studies have suggested that resident cardiac macrophages are slowly replaced by monocyte-derived populations[13]. However, our data suggest that cardiac macrophages must be stratified appropriately for full understanding of their life cycle. CCR2$^-$MHC-II^{lo}TIMD4$^+$LYVE1$^+$ macrophages have negligible monocyte input at steady state and even in chronically infarcted tissue. The identification of $Timd4$ and $Lyve1$ expression in resident macrophages from

other tissues suggests that they may represent important resident macrophage markers[38–40]. Specifically in the myocardium, TIMD4 and LYVE1 may be used to identify resident macrophages in the absence of dedicated tracking approaches. Given enough time, tissue cues may prompt recruited macrophages to ultimately express genes such as $Timd4$ and $Lyve1$. This possibility is evident based on adoptive transfer experiments in the peritoneum and lungs, where the tissue guides the identity of the transferred macrophage population[41,42]. Our study highlights the complexity and plasticity underlying recruited and resident cardiac macrophages at steady state and particularly within infarcted tissue. Greater understanding of this

dynamic process is required to delineate the probably differential contribution of individual macrophage subsets to tissue repair and injury, so that effective therapeutic strategies can be generated.

Online content

Any methods, additional references, Nature Research reporting summaries, source data, statements of data availability and associated accession codes are available at https://doi.org/10.1038/s41590-018-0272-2.

References

1. Lozano, R. et al. Global and regional mortality from 235 causes of death for 20 age groups in 1990 and 2010: a systematic analysis for the Global Burden of Disease Study 2010. *Lancet* **380**, 2095–2128 (2012).
2. Ismahil, M. A. et al. Remodeling of the mononuclear phagocyte network underlies chronic inflammation and disease progression in heart failure: critical importance of the cardiosplenic axis. *Circ. Res.* **114**, 266–282 (2014).
3. Epelman, S., Lavine, K. J. & Randolph, G. J. Origin and functions of tissue macrophages. *Immunity* **41**, 21–35 (2014).
4. Schulz, C. et al. A lineage of myeloid cells independent of Myb and hematopoietic stem cells. *Science* **336**, 86–90 (2012).
5. Epelman, S. et al. Embryonic and adult-derived resident cardiac macrophages are maintained through distinct mechanisms at steady state and during inflammation. *Immunity* **40**, 91–104 (2014).
6. Ginhoux, F. & Guilliams, M. Tissue-resident macrophage ontogeny and homeostasis. *Immunity* **44**, 439–449 (2016).
7. Porrello, E. R. et al. Transient regenerative potential of the neonatal mouse heart. *Science* **331**, 1078–1080 (2011).
8. Lavine, K. et al. Distinct macrophage lineages contribute to disparate patterns of cardiac recovery and remodeling in the neonatal and adult heart. *Proc. Natl Acad. Sci. USA* **111**, 16029–16034 (2014).
9. Aurora, A. B. et al. Macrophages are required for neonatal heart regeneration. *J. Clin. Invest.* **124**, 1382–1392 (2014).
10. Leid, J. M. et al. Primitive embryonic macrophages are required for coronary development and maturation. *Circ. Res.* **118**, 1498–1511 (2016).
11. Panizzi, P. et al. Impaired infarct healing in atherosclerotic mice with Ly-6C^{hi} monocytosis. *J. Am. Coll. Cardiol.* **55**, 1629–1638 (2010).
12. van Amerongen, M. J., Harmsen, M. C., van Rooijen, N., Petersen, A. H. & van Luyn, M. J. Macrophage depletion impairs wound healing and increases left ventricular remodeling after myocardial injury in mice. *Am. J. Pathol.* **170**, 818–829 (2007).
13. Molawi, K. et al. Progressive replacement of embryo-derived cardiac macrophages with age. *J. Exp. Med.* **211**, 2151–2158 (2014).
14. Serbina, N. V. & Pamer, E. G. Monocyte emigration from bone marrow during bacterial infection requires signals mediated by chemokine receptor CCR2. *Nat. Immunol.* **7**, 311–317 (2006).
15. Ridker, P. M. et al. Antiinflammatory therapy with canakinumab for atherosclerotic disease. *N. Engl. J. Med.* **377**, 1119–1131 (2017).
16. Hulsmans, M. et al. Macrophages facilitate electrical conduction in the heart. *Cell* **169**, 510–522 e520 (2017).
17. Miyanishi, M. et al. Identification of Tim4 as a phosphatidylserine receptor. *Nature* **450**, 435–439 (2007).
18. Clemente-Casares, X. et al. A CD103+ conventional dendritic cell surveillance system prevents development of overt heart failure during subclinical viral myocarditis. *Immunity* **47**, 974–989 (2017).
19. Van der Borght, K. et al. Myocardial infarction primes autoreactive T cells through activation of dendritic cells. *Cell Rep.* **18**, 3005–3017 (2017).
20. Gautier, E. L. et al. Gene-expression profiles and transcriptional regulatory pathways that underlie the identity and diversity of mouse tissue macrophages. *Nat. Immunol.* **13**, 1118–1128 (2012).
21. Tirosh, I. et al. Dissecting the multicellular ecosystem of metastatic melanoma by single-cell RNA-seq. *Science* **352**, 189–196 (2016).
22. Guilliams, M. et al. Unsupervised high-dimensional analysis aligns dendritic cells across tissues and species. *Immunity* **45**, 669–684 (2016).
23. Satpathy, A. T. et al. Zbtb46 expression distinguishes classical dendritic cells and their committed progenitors from other immune lineages. *J. Exp. Med.* **209**, 1135–1152 (2012).
24. Trapnell, C. et al. The dynamics and regulators of cell fate decisions are revealed by pseudotemporal ordering of single cells. *Nat. Biotechnol.* **32**, 381–386 (2014).
25. Chen, J., Schlitzer, A., Chakarov, S., Ginhoux, F. & Poidinger, M. Mpath maps multi-branching single-cell trajectories revealing progenitor cell progression during development. *Nat. Commun.* **7**, 11988 (2016).
26. Parkhurst, C. N. et al. Microglia promote learning-dependent synapse formation through brain-derived neurotrophic factor. *Cell* **155**, 1596–1609 (2013).
27. Yona, S. et al. Fate mapping reveals origins and dynamics of monocytes and tissue macrophages under homeostasis. *Immunity* **38**, 79–91 (2013).
28. Leuschner, F. et al. Rapid monocyte kinetics in acute myocardial infarction are sustained by extramedullary monocytopoiesis. *J. Exp. Med.* **209**, 123–137 (2012).
29. Leuschner, F. et al. Angiotensin-converting enzyme inhibition prevents the release of monocytes from their splenic reservoir in mice with myocardial infarction. *Circ. Res.* **107**, 1364–1373 (2010).
30. Nahrendorf, M. et al. The healing myocardium sequentially mobilizes two monocyte subsets with divergent and complementary functions. *J. Exp. Med.* **204**, 3037–3047 (2007).
31. Wan, E. et al. Enhanced efferocytosis of apoptotic cardiomyocytes through myeloid-epithelial-reproductive tyrosine kinase links acute inflammation resolution to cardiac repair after infarction. *Circ. Res.* **113**, 1004–1012 (2013).
32. Lim, H. Y. et al. Hyaluronan receptor LYVE-1-expressing macrophages maintain arterial tone through hyaluronan-mediated regulation of smooth muscle cell collagen. *Immunity* **49**, 326–341 e327 (2018).
33. Majmudar, M. D. et al. Monocyte-directed RNAi targeting CCR2 improves infarct healing in atherosclerosis-prone mice. *Circulation* **127**, 2038–2046 (2013).
34. Bajpai, G. et al. The human heart contains distinct macrophage subsets with divergent origins and functions. *Nat. Med.* **24**, 1234–1245 (2018).
35. Satoh, T. et al. Identification of an atypical monocyte and committed progenitor involved in fibrosis. *Nature* **541**, 96–101 (2017).
36. Menezes, S. et al. The heterogeneity of Ly6Chi monocytes controls their differentiation into iNOS+ macrophages or monocyte-derived dendritic cells. *Immunity* **45**, 1205–1218 (2016).
37. Ikeda, N. et al. Emergence of immunoregulatory Ym1(+)Ly6C(hi) monocytes during recovery phase of tissue injury. *Sci. Immunol.* **3**, eaat0207 (2018).
38. Mrdjen, D. et al. High-dimensional single-cell mapping of central nervous system immune cells reveals distinct myeloid subsets in health, aging, and disease. *Immunity* **48**, 599 (2018).
39. Han, X. et al. Mapping the mouse cell atlas by microwell-seq. *Cell* **172**, 1091–1107 e1017 (2018).
40. Mass, E. et al. Specification of tissue-resident macrophages during organogenesis. *Science* **353**, aaf4238 (2016).
41. van de Laar, L. et al. Yolk sac macrophages, fetal liver, and adult monocytes can colonize an empty niche and develop into functional tissue-resident macrophages. *Immunity* **44**, 755–768 (2016).
42. Gosselin, D. et al. An environment-dependent transcriptional network specifies human microglia identity. *Science* **356**, eaal3222 (2017).

Author contributions

S.A.D. and J.A.M. designed and performed experiments with the help of X.C-C., S.H., C.K., M.G.A., A.W., L.A., R.Z., R.B. and I.B. A.M. performed all surgeries. M.H., K.J.L., B.R., F.G., M.I.C. and C.S.R. provided expertise and feedback. S.N. performed the bioinformatics analyses. J.C. performed the Mpath analysis. S.E. conceived the study, obtained funding and wrote the manuscript with S.A.D., S.N. and J.A.M.

Competing interests

The authors declare no competing interests.

Additional information

Supplementary information is available for this paper at https://doi.org/10.1038/s41590-018-0272-2.

Reprints and permissions information is available at www.nature.com/reprints.

Correspondence and requests for materials should be addressed to S.E.

Publisher's note: Springer Nature remains neutral with regard to jurisdictional claims in published maps and institutional affiliations.

Methods

Mice. All mice used in this study were purchased from The Jackson Laboratory and were bred in our animal facility before use. All mice were bred and housed in a pathogen-free environment at the University Health Network Animal Facility and were fed standard rodent chow. All experimental procedures were approved by the Animal Care Committee of the Toronto General Research Institute and were performed according to the guidelines of the Canadian Council on Animal Care.

Fate mapping. To induce recombination in *Cx3cr1*[CreER–YFP]:*R26*[Td] mice, tamoxifen was administered via tamoxifen-containing chow (Envigo) for 11 d or injected into pregnant females at E18.5 via i.p. injection at 2 mg per mouse. For tamoxifen preparation, 100 mg of tamoxifen-free base (Sigma-Aldrich T5648) was added to 0.5 ml 95% ethanol; 9.5 ml corn oil was then added to the mixture and the mixture was vortexed and sonicated until the oil was dissolved.

Macrophage depletion. Diphtheria toxin (Sigma) was diluted in PBS and administered to mice i.p. acutely (500 ng daily for 3 consecutive days) or chronically (500 ng daily for 3 consecutive days, then 250 ng daily, 3× weekly for 2 additional weeks). For the long-term depletion and functional experiment, 500 ng diphtheria toxin was administered i.p. daily for the first 7 d, followed by 250 ng i.p. daily until 35 d after myocardial infarction.

Human samples. Human cardiac tissue samples were obtained from the Washington School of Medicine from subjects with end-stage cardiomyopathy during the time of implantation of the left ventricular assist device. Informed consent was received from all subjects and approved by the Washington University Institutional Review Board, with compliance to all relevant ethical regulations. After left ventricular apical core segment was removed, before placement of the inlet cannula, the cardiac tissue was immediately placed into cold RPMI medium. Human cardiac tissue was minced and digested in a fashion identical to that for mouse cardiac tissue.

Cell visualization. To visualize human macrophage subset cell morphology, hearts were harvested, digested and prepared for flow cytometry. Sorted cells (AriaIII-CFI BRVY) were cytospun onto slides and stained with Hema3 (Fisher Scientific). Cells were imaged with a Zeiss Axioscope at 20×.

Gene expression analysis. RNA from human cardiac macrophages was extracted from Trizol samples using the Qiagen micro-kit (Qiagen) as we previously described[4]. Total RNA concentration and quality was determined by Agilent 2100 Bioanalyzer (Agilent Technologies) according to the manufacturer's recommendations.

Transcriptional array. RNA transcripts were first amplified by WTA2 kit (Sigma Aldrich). Total RNA (1 ng) was amplified according to the manufacturer's protocol. cDNAs were chemically labeled with Kreatech ULS labeling kit (Kreatech Diagnostics). Per reaction, 2.5 μg of DNA was mixed with Kreatech labeling buffer and Kreatech Cy5-ULS[4]. The reactions were incubated at 85 °C for 15 min in the dark and placed on ice for 3 min. Labeled DNAs were purified with QIAquick PCR purification columns (Qiagen Sciences). Labeled DNAs were quantified on a Nanodrop spectrophotometer. Each labeled DNA (2 μg) was suspended in Agilent 2X Gene Expression hybridization buffer, Agilent 10X Blocking agent and Kreatech Kreablock. The hybridization solutions were applied to Agilent Human 4×44K V1 microarrays. Hybridization was carried out at 65 °C for 20 h. Washing procedures were carried out according to Agilent gene expression protocols. Slides were scanned on an Agilent SureScan microarray scanner to detect Cy5 fluorescence. Gridding and analysis of images were performed using Agilent Feature Extraction v10.7.3.1. Background-subtracted, log-transformed, quantile-normalized data were analyzed using analysis of variance (ANOVA) testing with contrasts (Partek GS, Partek). For exploratory analyses, we set the threshold at a two-fold change with an unadjusted $P = 0.001$.

Tissue isolation and cell-surface staining. Mice were killed by CO_2 inhalation. Hearts were perfused with 20 ml of cold PBS. Hearts, lungs, livers and brains were chopped finely and digested, while being shaken, for 1 h at 37 °C in DMEM containing collagenase I (450 U ml⁻¹), DNase I (60 U ml⁻¹) and hyaluronidase (60 U ml⁻¹) enzymes (all from Sigma)[30]. The digested material from heart, liver and brain was filtered through 40 μM filters and pelleted by centrifugation (400g for 5 min at 4 °C) in Hank's balanced salt solution (HBSS) supplemented with 2% bovine serum + 0.2% BSA. Red blood cells were lysed in ACK lysis buffer (Invitrogen) for 5 min at room temperature and resuspended in FACS buffer (PBS containing 2% FCS and 2 mM EDTA). Liver was filtered and resuspended in 40% Percoll. Brain was filtered and resuspended in 40% Percoll mixed on top of 80% Percoll. Pellets were resuspended, red blood cells were lysed and samples were resuspended as described above. Finally, blood was collected in syringes containing 50 μl heparin, red blood cells were lysed, and pellets were resuspended as described above. Single-cell suspensions were then labeled for cell-surface markers using antibodies listed below (in the 'Mouse antibodies' paragraph in the 'Flow cytometry gating strategy and antibodies' subsection). Cells were labeled in 50 μl FACS buffer

with 0.2 μl antibody per sample, with the exception of the antibody to CCR2 (5 μl), for 30 min at 4 °C. Cells were washed and resuspended in 400 μl FACS buffer to be analyzed by flow cytometry (BD LSRII-OICR BGRV). For more information about tissue isolation, digestion and flow cytometric analysis, please review uploaded video content (https://www.jove.com/video/58114/isolation-identification-extravascular-immune-cells)[43].

BrdU incorporation. For proliferation experiments, 2 mg of BrdU (Sigma) was injected i.p. at 2 h before organ harvest as described[5]. To detect intracellular BrdU, the BD Bioscience Cytofix/Cytoperm protocol was used. Cells were fixed after cell surface labeling, washed and resuspended with permeabilization buffer overnight. DNA was digested for 1 h with DNase (Sigma), cells were labeled with Fc receptor–blocking reagent for 15 min and were then labeled with an antibody to BrdU for 30 min.

Flow cytometry gating strategy and antibodies. After gating on CD45⁺ cells, doublets were excluded and live cells were analyzed using forward scatter (FSC) and side scatter (SSC) live-dead exclusion. Single cell analysis software (FlowJo) was used to analyze cell cytometric data.

Gating strategy (mouse). Cardiac macrophages were identified as CD45⁺CD11b⁺CD64⁺ and were further parsed by CCR2, MHC-II, Timd4, Lyve1 and Td. Infiltrating monocytes in the myocardium were identified as CD45⁺CD11b⁺CD64⁺Ly6C⁺. Blood monocytes were identified as CD115⁺CD11b⁺Ly6C⁺. Brain microglia were identified as CD45loCD11b⁺F4/80⁺CD64⁺. Liver macrophages were identified as CD45⁺F4/80⁺CD11b⁺MHC-IIhi. Neutrophils were identified as CD45⁺CD11b⁺CD64⁻Ly6G⁺. Lymphocytes were identified as CD45⁺CD64⁻CD11b⁻.

Gating strategy (human). Cardiac macrophages were identified as CD45⁺CD64⁺MerTK⁺CD14⁺ and were further parsed by CCR2 and HLA-DR.

Mouse antibodies. We used antibodies to CD45 (30-F11), CD64 (X54-5/7.1), CD11c (N418), MHC-II (AF6-120.1), CD11b (M1/70), Timd4 (RMT4-54), Ly6C (HK1.4), CD115 (AF598), Ly6g (1A8), F4/80 (CI:A3-1), CD4 (RM4-5); CD8a (53-6.7), CD3e (145-2c11) and BrdU (Bu20a), as well as TruStain CD16/CD32 FC Block (93).

Human antibodies. We used antibodies to CD45 (HI30), MerTK (2B10C42), CD14 (M5E2), CD64 (10.1), CCR2 (K036C2) and HLA-DR (L243).

All mouse and human antibodies listed above were purchased from Biolegend, with the exception of antibodies to CCR2 (475301, R&D Systems), Lyve1 (ALY7, eBiosciences) and B220 (RA3-6B2); BV421-SA (BD Biosciences). Antibody clones are provided in parentheses. For more details, see the Nature Research Reporting Summary.

Myocardial infarction model. All left anterior descending artery ligations were performed as described[44]. Briefly, after shaving of the chest and 2% isoflurane induction of anesthesia (0.8 L min⁻¹ oxygen), mice were intubated and ventilated with a pressure-control ventilator (Kent Scientific). The thorax and pericardium were opened, and using a 7-0 silk suture (Deknatel), the left anterior descending artery was ligated, the chest was closed, and the animal recovered with an immediate 0.1 mg kg⁻¹ subcutaneous injection of buprenorphine, followed by another injection 24 h later. Control mice are those with unopened chests.

Parabiosis. The lateral aspects of female donor mice (left) and recipient mice (right) were shaved and matching skin incisions were made from behind the ear to the tail of each mouse, as we previously described[5]. The subcutaneous fascia was dissected to create ~0.5 cm of free skin. The olecranon and knee joints were attached by a mono-nylon 5.0 suture (Ethicon) and the dorsal and ventral skins were attached by continuous suture. Animals recovered with an immediate 0.1 mg kg⁻¹ subcutaneous injection of buprenorphine followed by another injection 24 h later. Maintenance subcutaneous saline injections were given for 1 week as well as 3% neomyocin antibiotics for 2 weeks. Mice were joined for 2–6 months. The percentage chimerism for each macrophage subset was normalized to blood monocytes in the recipient mouse that originated from the donor and expressed as a percentage (Normalized chimerism (%) = (Donor cells in recipient (%) / Ly6Chi monocyte donor cells in recipient (%)) × 100).

Bone marrow chimeras. Adult wild-type mice (CD45.1) were sublethally irradiated twice with 628 cGy with 3 h in between. Chimeras were made with CD45.1 C57BL/6 hosts receiving ~5×10⁶ bone marrow cells from CD45.2 C57BL/6 mice (*Cx3cr1*creER–YFP:*R26*Td) on the day of irradiation. Irradiation was performed using a Gammacell 40 exactor. For shielded bone marrow chimeras, the same irradiation was performed with the addition of a 1 cm–thick lead shield covering the thoracic cavity of the mouse using an XRAD320 irradiator. All animals received 3% neomycin antibiotics for 2 weeks.

Cell sorting. Mouse hearts were isolated and enzymatically digested as described[5], with the inclusion of 1 mM flavopiridol in the digestion buffer. Digestions were

stopped after 20 min and cells were processed into a single-cell suspension on ice. Cells were labeled with CD45 magnetic beads (Miltenyi Biotec) and subsequently fluorescently tagged antibodies to CD45, CD64 and CD11b. Hematopoietic cells were positively enriched using the AutoMacs instrument (Miltenyi Biotec) and live macrophages (CD45+, CD64+, CD11b+ and DAPI−) were sorted on the Aria Fusion (BD Bioscience) under low pressure into DMEM containing 50% FCS for cell visualization and 10x Genomics single-cell RNA sequencing or into RLT buffer (Qiagen) for RNA extraction.

Immunofluorescence. Hearts were isolated at reported times after myocardial infarction and cut longitudinally. They were fixed in 4% paraformaldehyde overnight and followed by a 30% sucrose gradient overnight. Tissue was embedded in OCT medium (Sakura Finetek) and flash frozen in isopentane suspended in liquid nitrogen. Tissue was sectioned in 10-µm slices at two cutting levels. Sections were blocked for 1 h in a 50:50 solution of permeabilization block (5% bovine serum, 0.01% Triton X in PBS) and normal serum block (Biolegend). Sections were washed with PBS and the primary antibody was diluted in FACS buffer and added overnight at 4 °C in a hydrated chamber (rat anti-CD68 (FA-11; ThermoFisher); biotin anti-Lyve1 (ALY7; eBiosciences)). Sections were washed with PBS and were labeled with secondary antibody diluted in PBS for 1 h at 4 °C (goat anti-rat IgG1-FITC (RTK2071); goat anti-rat IgG-AF647 (Poly4054) Biolegend). For LYVE1 staining the TSA Fluorescein kit was used (PerkinElmer). Sections were mounted with SlowFade Diamond Antifade Mountant with DAPI (ThermoFisher) and imaged on the LSM700 confocal microscope at 20× or 40× with immersion oil (AOmacrophage, Advanced Optical Microscopy Facility, Princess Margaret Cancer Research Tower, Toronto, Canada). Five images were taken per heart in each of the remote (uninfarcted), peri-infarct and infarct zones. A section without the primary antibody, but labeled with the secondary IgG1 antibody, was used to control for background. All cells were counted blindly per field of view.

Echocardiography. Mouse echocardiography was performed using the VisualSonics Vevo 2100 System using 1% isofluorane anesthetic. Temperature was held constant at 37 °C and heart rate held between 450 and 500 beats min−1. Two-dimensional B-mode images were obtained in the long- and short-axis views. VevoLab program was used for Simpson's volume measurements. For ejection fraction calculation, the left ventricle was traced and divided into three segments (proximal, mid and distal), and the length of each segment was measured, in both diastole and systole, in triplicate. Measurements were made in a blinded fashion. Ejection fraction was obtained for both day 7 and day 28 post-myocardial infarction time points, and a delta was calculated between the time points. For fractional shortening and end diastolic volume calculations, interventricular septum diameter, left interventricular diameter and posterior wall diameter measurements were done in both diastole and systole, in triplicate. Uninfarcted control animals were used as a baseline.

Histology. Hearts were harvested on day 35 after myocardial infarction. They were cut longitudinally to include a four-chamber view of the heart and were fixed overnight in 10% buffered formalin. Hearts were then paraffin embedded and sectioned at two cutting levels at 8-µm thickness. After deparaffinization and rehydration steps, sections were stained with hematoxylin and eosin, Picrosirius Red or Fast Green (Chondrex) for fibrosis, or wheat germ agglutinin (Vector Labs) and mounted with SlowFade Diamond Antifade Mountant with DAPI (ThermoFisher) for cardiomyocyte hypertrophy. Slides were imaged using the Aperio AT2 slide scanner or the Olympus Fluorescence Upright microscope at 20× (Advanced Optical Microscopy Facility) in all three of the remote (uninfarcted), peri-infarct and deep-infarct zones. Fibrosis images were processed using Aperio ImageScope software and percentage fibrosis was quantified with ImageJ software. Wheat germ agglutinin images were processed using Metamorph software. All cardiomyocytes in cross-section were counted and measured per field of view on ImageJ. All measurements were made in a blinded fashion.

Statistics. All data are presented as mean ± s.e.m. Sample size estimates were based on the variance seen in our previously published work[5]. Student's t-test was used for comparisons between experimental groups (a two-tailed, unpaired test was used unless otherwise indicated). No randomization was used in this study. Significant differences were defined at $P < 0.05$. If multiple comparisons were used, a Bonferroni correction was used. Survival analysis was performed using a Kaplan–Meier plot using a log-rank (Mantel-Cox) test. All statistical analyses were done using Prism software.

Single-cell droplet experiments. A total of 1,780 cardiac macrophages and dendritic cells (1:1 ratio) for the macrophage-dendritic cell scRNA-seq experiment and 6,503 cardiac mononuclear cells for the control–myocardial infarction scRNA-seq experiment were sequenced to a read depth of ~130,000 reads per cell and run through the 10x Genomics cell ranger platform.

Single-cell suspensions were prepared as outlined by the 10x Genomics Single Cell 3′ v2 Reagent kit user guide. Briefly, samples were washed twice in PBS (Life Technologies) plus 0.04% BSA (Sigma). Each wash was performed with a 6 min centrifugation at 330g and resuspension in 1 ml PBS plus 0.04% BSA. Sample

viability was assessed using trypan blue (ThermoFisher) and a hemocytometer (ThermoFisher), and the appropriate volume for each sample was calculated. After droplet generation, samples were transferred onto a prechilled 96-well plate (Eppendorf), plates were heat-sealed and reverse transcription was performed using a Veriti 96-well thermal cycler (Thermo Fisher). After reverse transcription, cDNA was recovered using Recovery Agent provided by 10x Genomics followed by a Silane DynaBead cleanup (ThermoFisher) as outlined by the user guide. Purified cDNA was amplified and cleaned up using SPRIselect beads (Beckman). Samples were diluted at 4:1 (elution buffer (Qiagen)/cDNA) and run on a Bioanalyzer (Agilent Technologies) to determine cDNA concentration. cDNA libraries were prepared as outlined by the Single Cell 3′ Reagent kit v2 user guide with appropriate modifications to the PCR cycles based on the calculated cDNA concentration (as recommended by 10x Genomics).

Sequencing. The molarity of each library was calculated based on library size as measured by bioanalyzer (Agilent Technologies) and quantitative PCR amplification data (Kappa/Roche). Samples were pooled and normalized to 10 nM, and then diluted to 2 nM using elution buffer (Qiagen) with 0.1% Tween 20 (Sigma). Each 2 nM pool was denatured using 0.1 N NaOH at equal volumes for 5 min at room temperature. Library pools were further diluted to 20 pM using HT-1 (Illumina) before being diluted to a final loading concentration of 14 pM. Some 150 µl from the 14 pM pool was loaded into each well of an 8-well strip tube and loaded onto a cBot (Illumina) for cluster generation. Samples were sequenced on a HiSeq 2500 with the following run parameters: read 1, 26 cycles; read 2, 98 cycles; index 1, 8 cycles.

Single-cell RNA sequencing analysis. The sequenced data were processed into expression matrices with the Cell Ranger Single Cell software suite 1.3.1 by 10x Genomics (http://10xgenomics.com/). Raw base-call files from HiSeq2500 sequencer were demultiplexed into library-specific FASTQ files. Sequencing reads were aligned to the mouse transcriptome using STAR aligner[45]. Subsequently, cell barcodes and unique molecular identifiers underwent filtering and correction. Reads associated with the retained barcodes were quantified and used to build a transcript count table.

The standard procedures of filtering, variable gene selection, dimensionality reduction and clustering were performed using the scRNA-seq analysis R package Seurat (v.2.3.0)[46]. To exclude low-quality cells in both single-cell experiments, we filtered cells that expressed fewer than 200 genes per 1,000 unique molecular identifiers, and to exclude probable doublets, cells with >5,800 unique molecular identifiers were removed.

All genes that were not detected in at least three single cells were excluded. Based on these criteria, 12,916 genes across 1,590 samples in the macrophage-dendritic cell data set and 15,147 genes across 6,473 samples (1,783 control macrophages and 4,690 post-infarct macrophages) in the control-myocardial infarction data set remained for downstream analysis. To reduce biases caused by technical variation, sequencing depth and capture efficiency, normalization was performed using the deconvolution approach of Lun et al.[47] as implemented in R packages Scran (1.6.2)[47] and Scater (1.6.0)[48]. This normalization method pools expression counts from linear size groups of cells. These group-specific size factors are than deconvolved into cell-specific size factors that are used to scale the counts of individual cells.

The expression matrix underwent dimensionality reduction using principal component analysis. We first selected genes with high variance using the FindVariableGenes function with log-mean expression values between 0.06 and 2 for the macrophage-dendritic cell data set and 0.0125 and 1.5 for the control-myocardial infarction data, and dispersion (variance/mean) between 0.5 and 30 for both data sets. The number of highly variable genes based on these criteria were 1,344 genes for the macrophage-dendritic cell data set, and 1,242 genes for the control-myocardial infarction data set. Principal component analysis was performed on the selected variable genes and 15 and 20 significant principal components were identified for downstream analysis of the macrophage-dendritic cell and control-myocardial infarction data, respectively. The number of significant principal components to include in downstream analysis was determined based on the elbow point on the plot of standard deviations of principal components.

Clusters were identified by a graph-based clustering approach implemented by the FindCluster function in Seurat. Cells were embedded in a k-nearest neighbors graph based on the euclidean distance matrix constructed on the significant principal components. The Louvian modularity optimization algorithm[49] was applied to iteratively group cells together into clusters. We employed t-SNE for dimensionality reduction and visualization of our data sets.

The modularity-based clustering is a sensitive method that can occasionally overpartition larger clusters to detect rare populations. We therefore merged together very transcriptionally similar clusters (with no significant differential gene expression). In addition, two small clusters of contaminating B cells (enriched in *Cd79b, Cd79a, Ly6d* and *Ptprcap*) and stromal cells (enriched in *Sparc, Fabp4, Igfbp7* and *Crip2*) were removed from the control-myocardial infarction data set before any subsequent analysis.

For all single-cell differential expression tests, we used the model-based analysis of single-cell transcriptomics (MAST) test[50]. The MAST framework is a

two-part generalized linear model that parameterizes both the discrete expression rate of each gene across cells and the continuous expression level conditional on the gene being expressed. To define a unique expression profile for each cluster, differential expression was tested between each cluster and all other clusters combined. The MAST test as implemented in Seurat returns an "adj_pval" and an "avg_logFC" for each gene. The expression profile of each cluster's top 65 genes (based on avg_logFC) were visualized as a heatmap. Differential expression testing was also performed between two clusters, between control and post-infarct clusters and between overlapping and nonoverlapping clusters as specified in Fig. 4. See Supplementary Table 1 for differentially expressed genes between control and myocardial infarction samples found within overlapping clusters. See Supplementary table 2 for differentially expressed genes in each cluster found in post-infarct sample.

Pathway enrichment analysis. gProfiler (http://www.biit.cs.ut.ee/gprofiler/) [51] was applied to identify enriched pathways based on the differentially expressed genes between two groups. We used pathway gene sets from biological processes of Gene Ontology (http://www.geneontology.org/) and molecular pathways of Reactome (http://www.reactome.org/).

Single-cell trajectory analysis. We used Monocle v.2.8.0 (refs. [24,52]) to investigate inferred developmental trajectories between macrophage and monocyte subsets. Monocle uses reversed graph embedding to learn the sequence of gene expression changes that each cell undergoes within the dynamic biological sample provided. It than places each cell at an appropriate position along this trajectory of gene expression changes. The data, previously scaled, normalized and clustered by the Seurat tool, was loaded into a monocle object. Dimensionality reduction was performed using the reduceDimension command with parameters max_components = 2, reduction_method = "DDRTree". The trajectory was then built using the plot_cell_trajectory command with default parameters. Cells were sorted in pseudotime order and placed along a trajectory based on a priori found differentially expressed genes. For each trajectory analysis, we defined the cluster with higher expression of monocytic genes as the "root_state" (the starting point) of the trajectory. Changes in genes that are significantly branch dependent were visualized by a heatmap using plot_pseudotime_heatmap. The kinetic trend of the expression levels of significant genes through pseudotime was depicted by individual graphs using the plot_genes_in_pseudotime function.

The Mpath algorithm[25] was used as a secondary method for assessing developmental trajectories. Mpath constructs multibranching cell lineages and reorders individual cells along the branches. Scaled expression values of variable genes were extracted from Seurat pipeline and were used as input data to Mpath. The five clusters identified by Seurat were used as landmarks. Euclidean distance

was used to calculate dissimilarities between cells and landmarks. Tree trimming is done by using trim_net function with method mst.

Reporting Summary. Further information on research design is available in the Nature Research Reporting Summary linked to this article.

Code availability. R scripts for data processing are available through https://github.com/snejat/EpelmanLab_scRNAseq_Cardiac_Macrophages. There is no restriction on the use of the code or data.

Data availability

Single-cell sequence data that support the findings of this study are available through the National Center for Biotechnology Information Gene Expression Omnibus (NCBI GEO) (GSE119355). The Agilent gene array data that support the findings of this study are available through the NCBI GEO (GSE119515).

References

43. Aronoff, L., Epelman, S. & X, C.-C. Isolation and identification of extravascular immune cells of the heart. *J. Vis. Exp.* **138**, 7 (2018).
44. Noyan-Ashraf, M. H. et al. GLP-1R agonist liraglutide activates cytoprotective pathways and improves outcomes after experimental myocardial infarction in mice. *Diabetes* **58**, 975–983 (2009).
45. Dobin, A. et al. STAR: ultrafast universal RNA-seq aligner. *Bioinformatics* **29**, 15–21 (2013).
46. Butler, A., Hoffman, P., Smibert, P., Papalexi, E. & Satija, R. Integrating single-cell transcriptomic data across different conditions, technologies, and species. *Nat. Biotechnol.* **36**, 411–420 (2018).
47. Lun, A., McCarthy, D. & Marioni, J. A step-by-step workflow for low-level analysis of single-cell RNA-seq data with Bioconductor. *F1000 Res.* **5**, 2122 (2016).
48. McCarthy, D., Campbell, K., Lun, A. & Wills, Q. Scater: pre-processing, quality control, normalization and visualization of single-cell RNA-seq data in R. *Bioinformatics* **33**, 1179–1186 (2017).
49. Blondel, V. D., Guillaume, J. L., Lambiotte, R. & Lefebvre, E. Fast unfolding of communities in large networks. *J. Stat. Mech.* **10**, 10008 (2008).
50. Finak, G. et al. MAST: a flexible statistical framework for assessing transcriptional changes and characterizing heterogeneity in single-cell RNA sequencing data. *Genome Biol.* **16**, 278 (2015).
51. Reimand, J. et al. g:Profiler—a web server for functional interpretation of gene lists (2016update). *Nucleic Acids Res.* **44**, W83–W89 (2016).
52. Qiu, X. et al. Reversed graph embedding resolves complex single-cell trajectories. *Nat. Meth.* **14**, 979–982 (2017).

nature research

Corresponding author(s): Slava Epelman

Reporting Summary

Nature Research wishes to improve the reproducibility of the work that we publish. This form provides structure for consistency and transparency in reporting. For further information on Nature Research policies, see Authors & Referees and the Editorial Policy Checklist.

Statistical parameters

When statistical analyses are reported, confirm that the following items are present in the relevant location (e.g. figure legend, table legend, main text, or Methods section).

n/a	Confirmed	
☐	☒	The exact sample size (*n*) for each experimental group/condition, given as a discrete number and unit of measurement
☐	☒	An indication of whether measurements were taken from distinct samples or whether the same sample was measured repeatedly
☐	☒	The statistical test(s) used AND whether they are one- or two-sided *Only common tests should be described solely by name; describe more complex techniques in the Methods section.*
☐	☒	A description of all covariates tested
☐	☒	A description of any assumptions or corrections, such as tests of normality and adjustment for multiple comparisons
☐	☒	A full description of the statistics including central tendency (e.g. means) or other basic estimates (e.g. regression coefficient) AND variation (e.g. standard deviation) or associated estimates of uncertainty (e.g. confidence intervals)
☐	☒	For null hypothesis testing, the test statistic (e.g. F, t, r) with confidence intervals, effect sizes, degrees of freedom and P value noted *Give P values as exact values whenever suitable.*
☐	☒	For Bayesian analysis, information on the choice of priors and Markov chain Monte Carlo settings
☐	☒	For hierarchical and complex designs, identification of the appropriate level for tests and full reporting of outcomes
☐	☒	Estimates of effect sizes (e.g. Cohen's *d*, Pearson's *r*), indicating how they were calculated
☐	☒	Clearly defined error bars *State explicitly what error bars represent (e.g. SD, SE, CI)*

Our web collection on statistics for biologists may be useful.

Software and code

Policy information about availability of computer code

Data collection	10x genomics; BD FACSDIVA (v8.0.1)
Data analysis	Cell Ranger (v2.1); ImageJ (c1.48); Flowjo (v10); Vevolab (Seura1.7.2); Prism (v7) Seurat (v.2.3.0); Scran (V.1.6.2); Scater (v.1.6.0); Monocle 2; MPath; gProfiler (http://www.biit.cs.ut.ee/gprofiler/)

For manuscripts utilizing custom algorithms or software that are central to the research but not yet described in published literature, software must be made available to editors/reviewers upon request. We strongly encourage code deposition in a community repository (e.g. GitHub). See the Nature Research guidelines for submitting code & software for further information.

Data

Policy information about availability of data

All manuscripts must include a data availability statement. This statement should provide the following information, where applicable:
- Accession codes, unique identifiers, or web links for publicly available datasets
- A list of figures that have associated raw data
- A description of any restrictions on data availability

we have uploaded all the single cell RNA sequencing data (mouse) to the NCBI as requested (https://www.ncbi.nlm.nih.gov/geo/query/acc.cgi?acc=GSE119355). We have also uploaded our gene array data (human) to NCBI as well (https://www.ncbi.nlm.nih.gov/geo/query/acc.cgi?acc=GSE119515).

Field-specific reporting

Please select the best fit for your research. If you are not sure, read the appropriate sections before making your selection.

☒ Life sciences   ☐ Behavioural & social sciences   ☐ Ecological, evolutionary & environmental sciences

For a reference copy of the document with all sections, see nature.com/authors/policies/ReportingSummary-flat.pdf

Life sciences study design

All studies must disclose on these points even when the disclosure is negative.

Sample size	Sample size was determined during experimental design based on the type of measurements made (flow vs echocardiogram) and our extensive experience with data variation with each technique. A power calculation was not done.
Data exclusions	No data exclusions were performed following analysis. Mice were excluded from the study if a failed myocardial infarction surgery was determined. This exclusion criteria was predetermined.
Replication	All experiments were repeated with >2 independent experiments and all replications were reproducible.
Randomization	All mice for this study were randomized to make sure litter-mates were used in all experiments where possible.
Blinding	Blinding for experiments was accomplished by segregating treatment groups by ear tag number only. Data analysis was performed by a second investigator with no knowledge of the tags associated to treatment groups for all functional experiments.

Reporting for specific materials, systems and methods

Materials & experimental systems

n/a	Involved in the study
☒	Unique biological materials
☐	☒ Antibodies
☒	Eukaryotic cell lines
☒	Palaeontology
☐	☒ Animals and other organisms
☐	☒ Human research participants

Methods

n/a	Involved in the study
☒	ChIP-seq
☐	☒ Flow cytometry
☒	MRI-based neuroimaging

Antibodies

Antibodies used	Mouse antibodies used: CD45 (30-F11); Cat# 103126; Dilution 1:250 CD64 (X54-5/7.1); Cat # 139306; Dilution 1:250 CD11c (N418); Cat # 117334; Dilution 1:250 MHC-II (AF6-120.1); Cat # 116415; Dilution 1:250 CD11b (M1/70); Cat # 101222; Dilution 1:250 Timd4 (RMT4-54); Cat # 130009; Dilution 1:250 Ly6C (HK1.4); Cat # 128024; Dilution 1:250 CD115 (AFS98); Cat # 135505; Dilution 1:250 Ly6g (1A8) Cat # 127623; Dilution 1:250 F4/80 (CI:A3-1); Cat # 123124; Dilution 1:250 CD4 (RM4-5); Cat # 100536; Dilution 1:250 CD8a (53-6.7); Cat # 100708; Dilution 1:250 CD3e (145-2c11); Cat #100309; Dilution 1:250 BrdU (Bu20a); Cat # 339812 ; Dilution 1:25 TruStain CD16/CD32 FC Block (93). Cat # 101320; Dilution 1:100 CD68 (FA-11); Cat #137001; Dilution 1:100 Human Antibody used: CD45 (HI30); Cat # 304028; Dilution 1:250 MerTK (2B10C42); Cat #367603; Dilution 1:250 CD14 (M5E2); Cat # 301806; Dilution 1:250 CD64 (10.1); Cat #305005; Dilution 1:250

CCR2 (K036C2); Cat # 357207; Dilution 1:250
HLA-DR (L243). Cat # 307626; Dilution 1:250

All antibodies listed above were purchased from Biolegend with the exception of
CCR2 (475301) (R&D Systems); Cat #FAB5538A; Dilution 1:10
Lyve1 (ALY7) (eBiosciences); Cat # 13-0443-82; Dilution 1:250 (flow); Dilution 1:100 (IF)
B220 (RA3-6B2); Cat # 553088; Dilution 1:250
BV421-SA (BD Biosciences); Cat # 563259; Dilution 1:200

Validation	All antibodies were validated by us using appropriate FMO/isotype controls for flow cytometry. All antibodies had validation statement provided on the website of the manufacturer.

Animals and other organisms

Policy information about studies involving animals; ARRIVE guidelines recommended for reporting animal research

Laboratory animals	Mice: both male and female mice were used. Ages are specified for each experiment. All mice ordered from Jackson Laboratory. Strains: C57BL/6 (#000664); CCR2KO (#004999); RosaTd (#007914); RosaDTR (#007900); Cx3cr1-CreER-YFP (#021160); Cx3cr1-CreER (#020940);
Wild animals	Wild animals were not used.
Field-collected samples	*For laboratory work with field-collected samples, describe all relevant parameters such as housing, maintenance, temperature, photoperiod and end-of-experiment protocol OR state that the study did not involve samples collected from the field.*

Human research participants

Policy information about studies involving human research participants

Population characteristics	Human cardiac tissue samples were obtained from the Washington School of Medicine from patients with end-stage cardiomyopathy during the time of implantation of the left ventricular assist device. Informed consent was received from all patients and approved by the Washington University IRB panel. After LV apical core segment was removed, prior to placement of the inlet cannula, the cardiac tissue was immediately placed into cold RPMI media. Patients had end-stage cardiomyopathy, from an ischemic etiology. There was no additional co-variate information provided for these samples
Recruitment	Pilot study, n=6 patient. These patients were recruited while in hospital awaiting LVAD implantation by a nurse coordinator. The only exclusion criteria was active infection or immunosuppressive medications. There were no obvious study selection biases that would have influenced the results except for the sample size (n=6), thereby increasing variability.

Flow Cytometry

Plots

Confirm that:

☒ The axis labels state the marker and fluorochrome used (e.g. CD4-FITC).

☒ The axis scales are clearly visible. Include numbers along axes only for bottom left plot of group (a 'group' is an analysis of identical markers).

☒ All plots are contour plots with outliers or pseudocolor plots.

☒ A numerical value for number of cells or percentage (with statistics) is provided.

Methodology

Sample preparation	Mice were sacrificed by CO2 inhalation. Hearts were perfused with 20mL of cold PBS. Hearts, lungs, livers, and brains were chopped finely and digested, while shaking, for 1hr at 37°C in DMEM containing collagenase I (450 U/mL), DNase I (60 U/mL), and hyaluronidase (60 U/mL) enzymes (all Sigma)12. The digested material from heart, liver and brain was filtered through 40uM filters and pelleted by centrifugation (400xg for 5min at 4°C) in HBSS supplemented with 2% bovine serum + 0.2% BSA. Red blood cells (RBCs) were lysed in ACK lysis buffer (Invitrogen) for 5min at room temperature and resuspended in FACs buffer (PBS containing 2% FCS and 2mM EDTA). Liver was filtered and resuspended into 40% Percoll. Brain was filtered and resuspended into 40% Percoll mixed over top of 80% Percoll. Pellets were resuspended, RBCs were lysed, and samples were resuspended as above. Finally, blood was collected in syringes containing 50 L heparin, RBCs were lysed, and pellets were resuspended as above. Single-cell suspensions were then stained for cell-surface markers using antibodies listed in the 'antibodies used' section. Cells were stained in 50uL FACS buffer with 0.2uL antibody per sample, with the exception of 5 L of CCR2 antibody, for 30min at 4°C. Cells were washed and resuspended in 400uL FACs buffer to be run by flow cytometry
Instrument	BD LSRII-OICR BGRV
Software	FlowJo
Cell population abundance	Sorted MFs represented ~1% of the total cell population from heart tissue samples. Purity was determined by flow cytometry

Cell population abundance [and confirmed in our data analysis.]

Gating strategy [For all experiments an initial gaiting strategy was used to gait on live (based on SSC-A/FSC-A) cells followed by two double exclusion gates (FSC-W/FSC-H and SSC-W/SSC-H) and a total CD45+ gate. Subsequent gates are defined in the figures/figure legends.]

☒ Tick this box to confirm that a figure exemplifying the gating strategy is provided in the Supplementary Information.